

Contents lists available at ScienceDirect

# Acta Materialia

journal homepage: www.elsevier.com/locate/actamat





# The role of embedded coordinates for disclinations and disconnection components

John P. Hirth a,1,\*, Jian Wang b,\*

- a Green Valley, Arizona 85614, USA
- <sup>b</sup> Mechanical and Materials Engineering, University of Nebraska-Lincoln, Lincoln, NE 68588, USA

#### ARTICLE INFO

Keywords: Disclination Disconnection Dislocation Boundary

#### ABSTRACT

The standard model is applied for partial disclination pairs in hard materials. These defects comprise two partial disclinations and an intervening fault that can be a twin boundary, grain boundary or interphase boundary. In three dimensions there are six types. Two of them can be considered Somigliana disclinations. The standard model includes geometrically nonlinear embedded coordinates. It entails partitioning of displacements that result in configurations and strain fields not considered classically for partial disclinations. These concepts are applied to boundary junctions, disconnections, and multiple twins. Recovered stress-free structures are considered.

#### 1. Introduction

The continuum theory for straight disclinations originated with the work of Volterra [1] and Somigliana [2]. The theory was augmented in [3]. The relation to crystalline defects came later in [4–7]. Both aspects are reviewed in [8–10]. The coherency disclination has been added recently [11]. The theory usually begins with Mura [12] and deWit [13] and use dislocation fields as Green's function kernels for integral solutions, a method that is followed here. There is a large literature on the linear elastic theory of disclinations as reviewed in [9,10]. We use these results but focus here on disclinations as represented in the standard model [14]. The paper is not a review of disclination theory. The model differs from the traditional one in that it entails embedded coordinates fixed on lattice sites, includes crystal symmetry, and is nonlinear geometrically.

A perfect disclination is a line defect for which there is a characteristic rotational gap. The associated elastic strains are so large that perfect disclinations are very rare as isolated defects in elastically hard metallic, ionic, and covalent materials. Partial disclination pairs (PDs), consisting of two partial disclinations and an intervening fault, do exist and are considered here. The faults entail surface defects such as subgrain, grain or twin boundaries, or interphase interfaces (such as coherent boundaries). Partial disclinations have been considered in [15–18]. The PDs were called generalized disclinations in [17,18] but what is generalized

is not the structure but the theory.

In this paper, we treat fault planes, the partitioning of elastic and plastic displacements and distortions, arrays of PDs, the disclination content of twinning disconnections, multipolar arrays of disclinations, recovery of strain fields at disclinations, and PDs in phase transformations. In what follows, we treat mainly wedge PDs although the same methods apply for other disclination types.

# 2. Partial disclination methodology

There are two descriptions of the faults in PDs. In the traditional extended disclination model, the fault is a perfect boundary with a rotational discontinuity, as for a twin boundary or a coherent terrace. The dislocation model of the fault is a set of dislocations with spacing d and a total dislocation content  $n\mathbf{b}$ . For distances from the PD greater than the fault width, the field is identical to that of a super-dislocation. Close to the PD the strain field deviates from that of a dislocation. The PD is equivalent to an extended super-dislocation. The quantity  $n\mathbf{b}$  is independent of d. In the limit the dislocations are continuous infinitesimal Bilby dislocations [19,20] and the result is identical to the perfect fault for the PD.

E-mail addresses: jbirsci8@gmail.com (J.P. Hirth), wangj6@gmail.com, jianwang@unl.edu (J. Wang).

<sup>\*</sup> Corresponding authors.

<sup>&</sup>lt;sup>1</sup> Retired

#### 2.1. Extended coordinates for PDs

There are two ways that embedded coordinates influence defect structures. The first is the elastic field. In linear elastic analyses for which the strain is assumed to be infinitesimal, there is no distinction whether the coordinates are the undeformed coordinates prior to the introduction of the dislocation or the deformed coordinates arising from it. Therefore, there is no shift in the origin of a displacement accompanying deformation. For a crystal lattice, one resolves this issue by imposing crystal symmetry and using embedded (Lagrangian) coordinates fixed on atom sites. This is the standard model (SM) [3]. The embedded and laboratory coordinates then differ because the embedded lattice sites shift as a result of local strain, whereas they do not in linear elasticity. The use of the embedded coordinates in the standard model is a nonlinear geometrical effect.

The second is the topological model (TM) of interfaces. The TM [20] was developed to describe complex defects such as disconnections and disclinations as a combination of the topological theory of Pond [21] and the structural definition of a disconnection [22]. The TM adopts embedded coordinates and partitioned displacements to satisfy

symmetry requirements. Defect characteristics are described by circuits in the dichromatic pattern, the superposition of the matrix and twin with a common origin, on a twin plane for example. The circuits reduce to translation vectors t in the dichromatic pattern. The TM was developed to describe complex defects such as disconnections and disclinations as a combination of the topological theory of Pond [21] and the structural definition of a disconnection [22]. It is topological in the limited geometrical sense of using embedded coordinates, consistent with general topological theory.

We select a type I twin to demonstrate the model. Fig. 1(a) shows a wedge PD described in the dislocation representation by crystal symmetry, leading to the partitioning of the displacements. The sense vector  $\boldsymbol{\xi}$ , coordinates x, y, z, and unit vectors  $\boldsymbol{i}$ ,  $\boldsymbol{j}$ ,  $\boldsymbol{k}$  are depicted. These are used throughout the paper unless otherwise noted. Fig. 1(b) shows the displacements associated with the usual model of insertion of a wedge on the right and removal of a wedge on the left. Fig 1(c) displays the overall displacement vectors  $\boldsymbol{f}$ , the overall rotations  $2\Delta\theta$ , and the associated Frank vectors:

$$\omega = 2\Delta\theta k \tag{1}$$

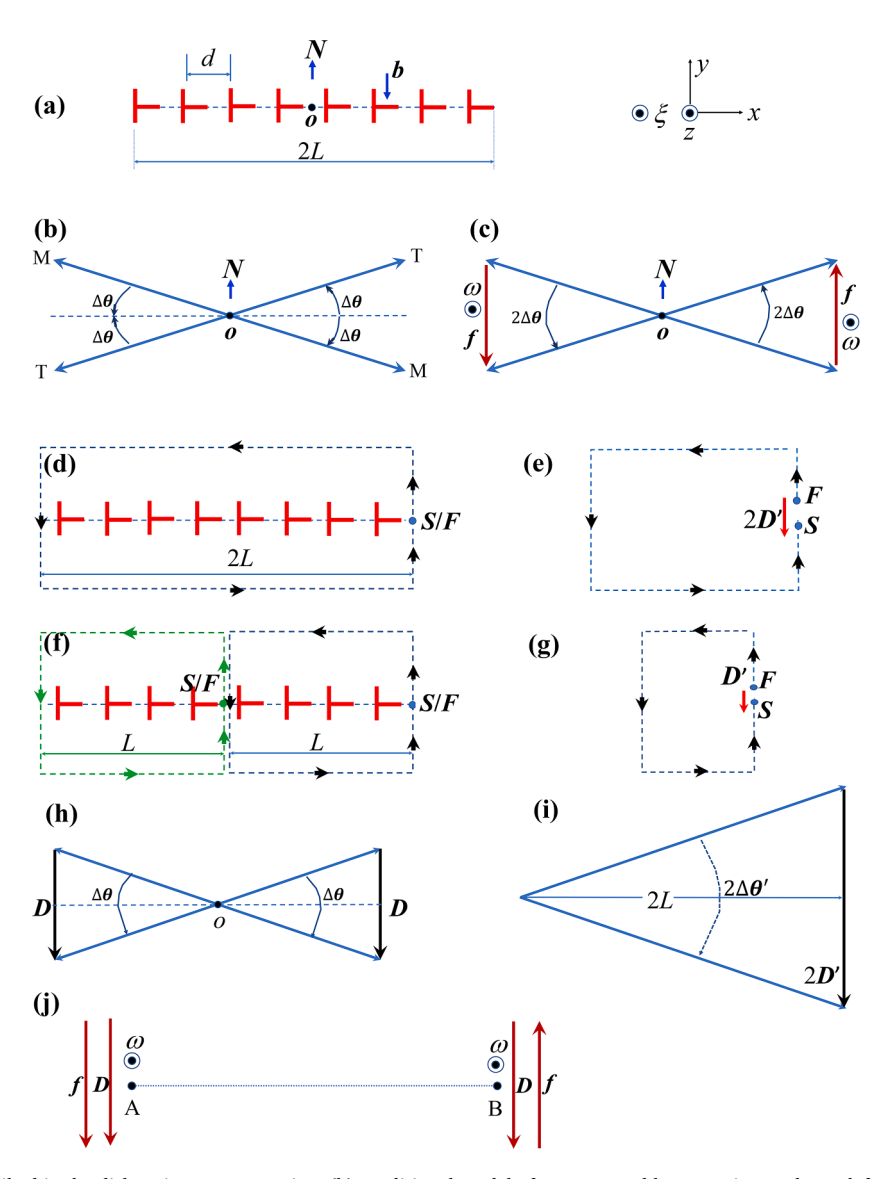


Fig. 1. (a) A wedge PD described in the dislocation representation. (b) Traditional model of a PD created by removing wedge at left and inserting one at right. The  $\Delta$  notation [9]. (c) The overall displacement vectors  $\mathbf{f}$ , the overall rotations  $2\Delta\theta$ , and the associated Frank vectors for the PD in (a). (d) ED represented as an edge dislocation array enclosed by a circuit. (e) FS/RH circuit in perfect reference crystal. (f). Partitioned circuit with origin at midpoint. (g). FS/RH circuit in reference crystal. (h). Overall changes in angle. (i) Equivalent of (h) for the traditional case. (j). Simple representation of vectors.

A local closed circuit, right-handed relative to the sense vector  $\boldsymbol{\xi}$ , is constructed in Fig. 1(d). The same circuit in a perfect reference crystal, shown in Fig. 1(e), has a closure vector  $\boldsymbol{FS}$  equal to the disclination vector  $\boldsymbol{2D'}$ : the  $\boldsymbol{FS/RH}$  convention. For either a continuum or for many high symmetry crystals, this procedure does not satisfy the  $\overline{2}$  symmetry in the  $\boldsymbol{y}$ -direction. In the SM, symmetrical partitioning is applied. Two circuits are introduced relative to the origin  $\boldsymbol{o}$  as in Fig. 1(f), as shown in Fig. 1(g), each has a disclination vector  $\boldsymbol{D'}$  and symmetry is satisfied. The far field is again equivalent to that of a super-dislocation  $\boldsymbol{B}$ , but this is misleading. The near field of the singularities varies markedly from that of a dislocation.

The reason for the difference between D and D' is seen in Fig. 1(h) and (i). With the symmetric arrangement in Fig. 1(h), the magnitude of D is:

$$D = (L/2) \tan(2\Delta\theta) \tag{2}$$

If instead one chose the origin at the left, as in Fig. 1(i), the closure magnitude would be:

$$D' = L \tan(\Delta \theta') \tag{3}$$

This result is correct linearly, but agrees with Eq. (2) only in the infinitesimal limit that r approaches  $\infty$ . Thus, both give the superdislocation B, but only the TM gives a precise D. The PD characteristic vectors are shown in Fig. 1(j) and (k). These include the Frank vector  $\omega$ , of use as a continuity vector. The vector  $\omega$  represents the crystallographic rotation across the twin plane. In Fig. 1, the local circuits terminate at  $\pm L$  so that D relates directly to  $2\Delta\theta$  and  $\omega$ . Each is a parallel indication of the strength of the PDs. A circuit for x>L would have a varying closure vector and after a St. Venant distance  $\approx 2L$  would become the constant B.

Also of interest is the rotational component  $\Delta\theta_T$  of the plastic deformation that creates the twin., which can analogously be expressed as the vector  $\Omega$ :

$$\mathbf{\Omega} = 2\Delta\theta_T \mathbf{\xi} \tag{4}$$

If the mechanism of twinning involves only one twinning disconnection (TD), e.g., one with the Burgers vector  $\mathbf{A}\boldsymbol{\delta}$  for a twin in face center cubic structure, then  $\boldsymbol{\omega}=\Omega$ . However, growth or annealing twins in Cu [23] are formed by successive sets of TDs,  $\mathbf{A}\boldsymbol{\delta}$ ,  $\mathbf{B}\boldsymbol{\delta}$ ,  $\mathbf{C}\boldsymbol{\delta}$ , with the same  $\boldsymbol{\omega}$ , but with  $\boldsymbol{\Omega}=0$ .

# 2.2. PD pairs and dipoles

There is a minor issue with the nomenclature for a PD, related to the formation proves in Fig. 2. Li [24] called the PD a dislocation wall and related it to what he called a disclination dipole. That terminology has been followed in many works, historical [25] and recent as reviewed in [9]. DeWit [26] defined two types of dipoles, a PD and a pair of opposite sign PDs. Thus, there is an ambiguity in terminology. The formation process [16,24,25] is nicely displayed in [9]. The notation in Fig. 2(a) is related to the dislocation version in Fig. 2(b). Two opposite sign PDs AB and CD, a dipole, are superposed as in Fig 2(b), cancelling the rotations to the right of *B*. The result in Fig. 2(c) is the PD extending from *E* to *F*. The result is simply to shorten the original PD. In terms of the relaxed, equilibrium elastic displacements, the addition of the negative **D** for CD (or  $\omega$ , or  $\Delta\theta$ ) in Fig. 2(b) results in a positive **D** (or  $\omega$ , or  $\Delta\theta$ ) for the right PD in EF. Instead, the notation in Fig. 2(a) refers to the sign of the imposed plastic wedge displacements f. Because of the symmetrical origin, the PD vectors  $\mathbf{D}$ ,  $\boldsymbol{\omega}$ , and  $\Delta \boldsymbol{\theta}$  all have the same sign, and the singularities have the same sign strain fields, so calling a PD a dipole is at variance with the terminology for dislocations and all other physical dipoles such as electron-hole pairs. Fig. 2(f), a version of that in [9], illustrates the incongruity. The addition of two like-sign super-dislocations **B** eliminate the long-range field, so Fig. 2(f) would have two dislocations constituting a monopole canceling a disclination dipole.

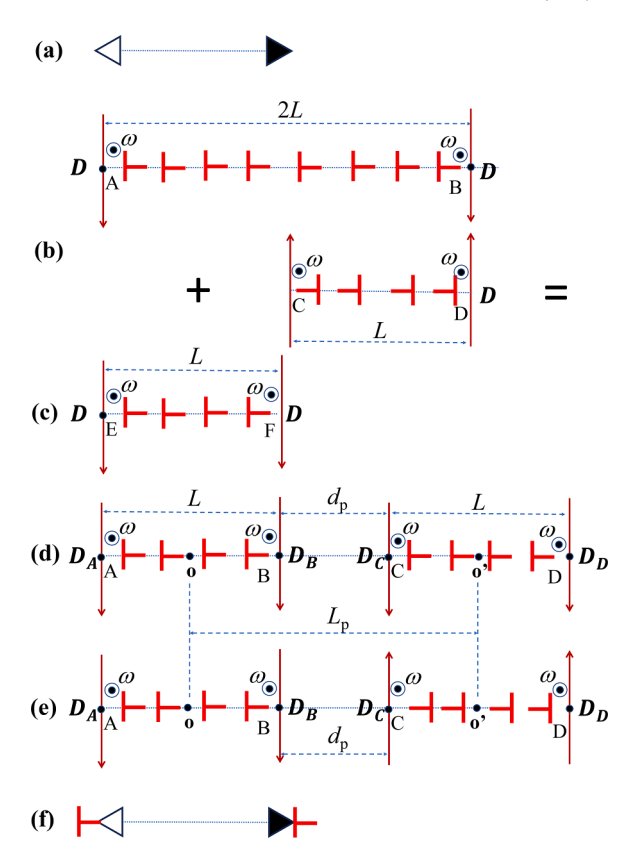


**Fig. 2.** (a). Traditional view of a PD. (b). Formation of a PD by the superposition of opposite sign partials. (c) Resultant PD. (d)Like-sign pair of PDs. (e) Opposite-sign pair of PDs. (f). PD dipole with long range field canceled by a dislocation pair constituting a monopole.

Here, we recommend calling the two PDs in Fig. 2(d) a like-sign partial pair and reserving the name dipole for interactions between opposite sign PDs, as in Fig. 2(e). The latter is DeWit's second case. The description in Fig. 2(a) is correct, but it is not a conventional dipole. We know of no examples, but a perfect disclination could dissociate into partial disclinations: a Cauchy cut could be constructed. In this example the rotation would tend to be suppressed on the intervening cut but added outside the cut.

Both the dipoles and the like-sign pairs in Fig. 2 are unstable with respect to out-of-plane displacement. The long-range field of a perfect wedge disclination dipole in Fig. 3(a) would be stable when the two disclinations are aligned at 45°, exactly like a dislocation dipole [14]. At short range, the interaction force increases in magnitude and the stable angle is less as in Fig. 3(b). At long range, the equilibrium position is shown in Fig. 3(c). The similar arrangement for short-range interactions is presented in Fig. 3(d). A lattice dislocation is attracted to the end of an PD as in Fig. 3(e), extending it, with the decrease in energy. Similarly, if there is a gap between repelling, like-sign PDs, lattice dislocations are attracted to fill the gap. The same is true for the filling of a spacing defect.

# 2.3. The mechanism of forming a PD

The mechanism of formation of the PD at twin plane is depicted in Fig. 4 [27]. TDs glide to create the interface, whether formed by the glide of lattice dislocations from the matrix,  $b_{gM}$ , or the twin,  $b_{gT}$  or both: the latter is shown in Fig. 4(a). Once the glide dislocations are in the boundary, as in Fig. 4(b), they rearrange to form the symmetrical array in Fig. 4(c). The separate vectors are inclined to the boundary normal by  $\omega/2$ . The in-plane coherency components of the lattice dislocations cancel, and the remaining leaving the unit, tilt, interface dislocations. In

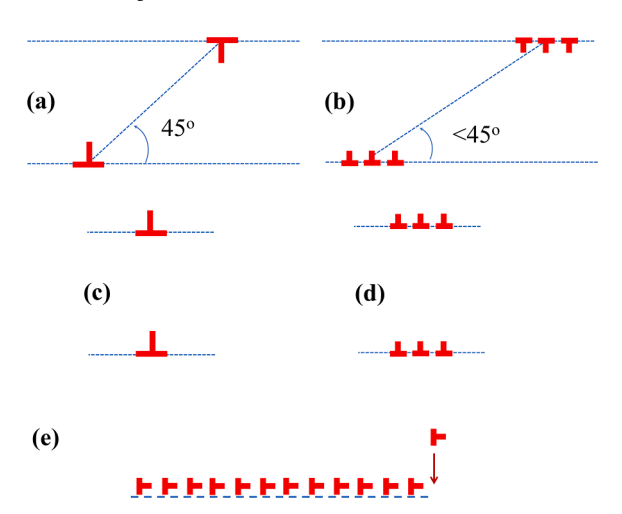


**Fig. 3.** (a). Stable position with respect to *y* displacements for a perfect coherency disclination dipole. (b). Equivalent for a PD dipole. (c) Equivalent for two like-sign perfect coherency disclinations. (d). Equivalent for two like-sign coherency PDs. (e) Lattice dislocation attracted to the end of a wedge PD.

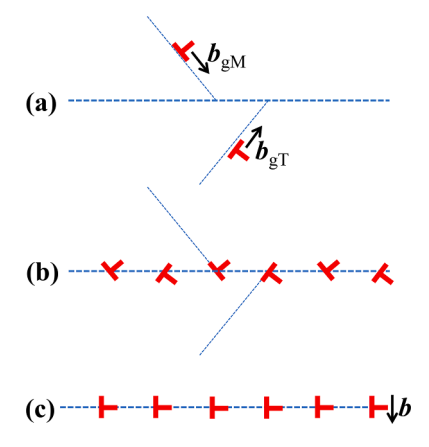


**Fig. 4.** (a). Lattice dislocations glide to create the interface, whether formed by the glide of lattice dislocations from the matrix,  $b_{gM}$ , or the twin,  $b_{gT}$  or both. (b). In-plane coherency components of the glide dislocations, inclined by the tilt angle  $2\alpha$ , cancel, leaving the unit, tilt, interface dislocations b in (c).

principle the PD could be formed by the climb of the interface dislocations, but this is a much more unlikely mechanism.

When dislocations enter from one side, the relaxed elastic displacements must partition so that the resultant boundary remains symmetrical and strain free. This is a key feature of the TM. For low-angle boundaries, the lattice is bent locally [28] and the partitioning occurs spontaneously. For intermediate angles the partitioning is achieved by a small amount of glide of the tilt dislocations. For high-angle boundaries, the simplest mechanism is symmetrical glide as in Fig. 4(a). Other cases still require simulation studies to determine the details.

# 2.4. Inhomogeneous extension

The above analysis applies for unconstrained equilibrium interfaces in the SM. Several situations still entail partitioning, but it is unequal. For an embedded twin with associated incompatibility strains, similar to an Eshelby inclusion [29], the compatibility strains are partitioned to the smaller crystal [30]. Analogously, when the elastic constants differ, the remote distortion strain is greater for the material with softer elastic constants for both the anisotropic elastic [31,32] and orthotropic elastic cases [33]. An important consequence is that the vector  $\omega$  still describes continuity [34]. This agrees with Frank [35] in that any shaped interface

can be constructed by a cut-and-paste process.

# 3. Types of DS

# 3.1. Straight PDs

Fig. 5 shows the three types of straight PDs described in [1,9,10] together with the associated fault planes. A negative wedge partial is shown in Fig. 5(a). The defect is characterized by a tangential imposed (or plastic) displacement with magnitude  $u_{\theta} = r\delta\theta$  in the isotropic elasticity approximation. In vector form, the imposed displacement  $u = (0, u_{\theta}, 0)$  diverges with r, and is related to the rotation vector  $\omega$  by the following:

$$u = r(\boldsymbol{\omega} \times \boldsymbol{i}) \tag{5}$$

Here,  $\omega=\Delta\theta$  **k**, and  $\mathbf{k}=\xi$ . If a through defect extending to free surfaces, the long-range elastic distortion is a pure rotation.

A twist disclination is shown in Fig. 5(b), another of Volterra's partials [1]. The screw-glide partial has an equivalent array of like sign screw dislocations, right-handed here. The imposed displacement  $u = (0, 0, u_z)$ , which diverges with r, is given by the following:

$$u = r(\omega \times i) = f \tag{6}$$

with  $\omega=\Delta\kappa j$ , and with j a unit vector in the  $\theta$  direction. The angle  $\Delta\kappa$  is the characteristic angle of rotation of the disclination in the fault plane with y as the z axis. In this case, the Burgers vector is z0 (0,0,z0). The distortion field of a through defect is a superposed rotation and shear strain. Two orthogonal twist partials comprise a spin disclination, with a pure rotation of the fault. There is an issue with the name for this PD. Historically it was given the present definition, including the naming of the defect [36]. Later, as in the reviews in [9,10] it was used for the orthogonal sets of PDs in a twist boundary, described in the next section. Here we retain the Volterra description and describe the orthogonal set

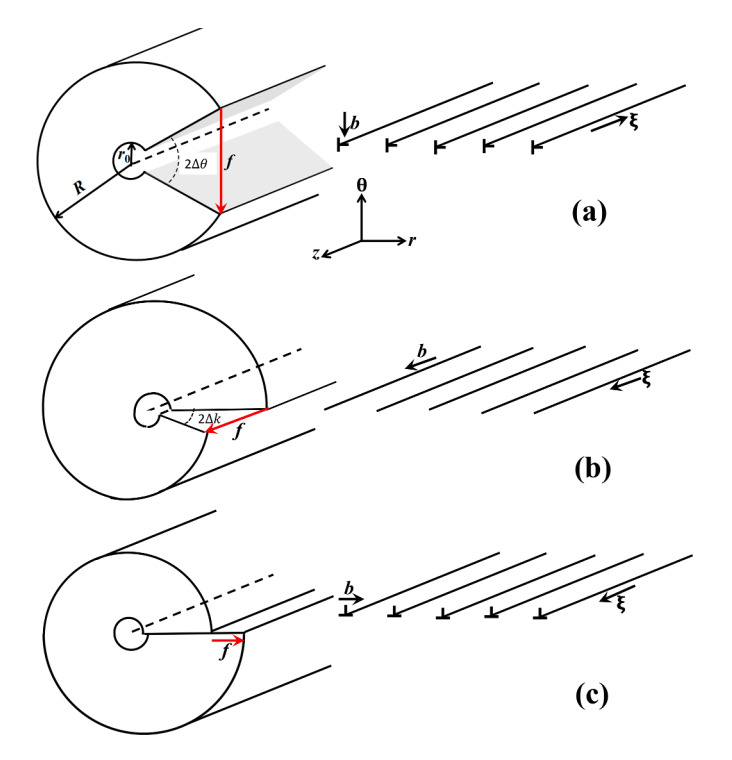


**Fig. 5.** Three types of straight partial disclinations and equivalent dislocation array. Displacement vectors f, and dislocation Burgers vectors are shown. Partial A is a partial wedge disclination with opening angle  $2\Delta\theta$ . Partial B is a partial twist disclination with opening angle  $2\Delta\kappa$ . Partial C is a partial coherency disclination.

as a spin disclination [37].

The edge-glide partial is shown in Fig. 5(c). It also can be either a coherency partial or a one-dimensional misfit partial. For the edge glide disclination, the displacement  $u = (u_{xx}, 0, 0)$  is:

$$u = \Delta r i \tag{7}$$

with i a unit vector in the r direction. The magnitude of the field is represented by  $\Delta r$ , which diverges with r. In this case, the Burgers vector is  $b=(b_r,0,0)$ . The atomic configurations are symmetrical in the x and y directions. Local one-dimensional coherency stresses are associated with the fault for this case. To first order, there is no long-range rotation for the coherency disclination, although second-order elastic rotations can be associated with coherency stresses (Poisson and nonlinear effects).

While not common, secondary PDs are possible. An example is the dissociation of a 1/6[112] partial bounding a (111),  $\Sigma$ 3 twin in fcc Al into a pair of 1/6 < 110> partials bounding a (110),  $\Sigma$ 9 twin [21]. Such PDs also are present at twin junctions [38].

The recent modification of the elastic field of a dislocation [38] entails the addition of a line force f to the traditional field. This suggests that line force partial pairs might be of future interest. This would add three more linear types. Two would be plane-strain defects with orthogonal f vectors and the other would be an anti-plane-strain defect with f parallel to  $\xi$ .

# 3.2. PD arrays

The corresponding two-dimensional PDs are shown in Fig. 6. Three disclinations are added to the three Volterra types. Fig. 6(a) is a wedge PD. The PD can end at free surfaces in the z direction. If terminated within a crystal, the Bilby or discrete dislocations must satisfy the continuity axiom. They can continue as out-of-plane segments as at a junction. Alternatively, they could continue as partitioned, symmetrical in-plane super-dislocations. This duality extends to Fig. 6(b) and (c). The  $2\Delta\theta$  rotation is in the (x, y) plane. The screw glide PD is depicted in Fig. 6

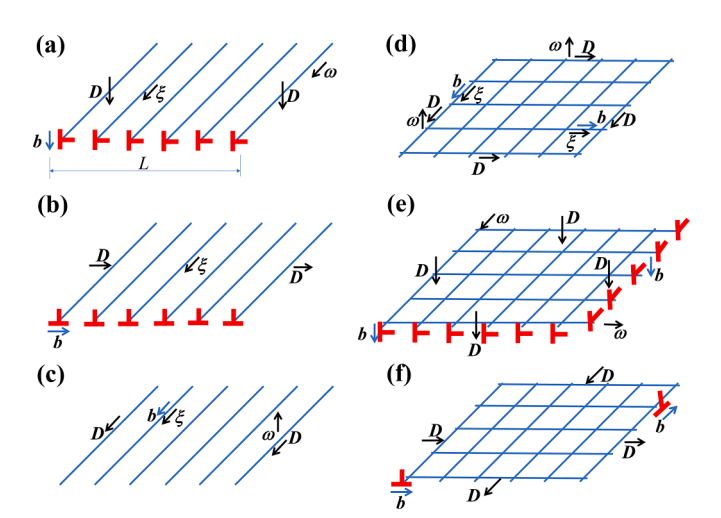


**Fig. 6.** Six two-dimensional types of PDs with vectors  $\textbf{\textit{D}}$  and dislocation analogs, with Burgers vectors  $\textbf{\textit{b}}$ . We show discrete dislocations, but the figures also apply for infinitesimal dislocation, (a). A wedge PD with characteristics  $\textbf{\textit{b}}$ ,  $\textbf{\textit{\xi}}$ ,  $\textbf{\textit{D}}$ ,  $\omega$ , and  $2\Delta\theta$ . (b). An edge-glide PD with a single array of edge dislocations. (c). A screw-glide PD with right-handed screw dislocations and a characteristic angle  $2\Delta\kappa$ . (d). A spin disclination with two sets of orthogonal screw dislocations. (b). An edge-glide PD with a single array of edge dislocations. (e). A skew edge PD with two orthogonal tilt arrays of edge dislocations in the fault plane. Figs. (a)–(c) are Volterra PDs, while Figs. (d)–(f) are pairs of Volterra disclinations. The dislocations cannot terminate within a crystal. They could terminate at free surfaces or as summed defects at the periphery. For (a)–(d), the result would be super-dislocations at the ends. For (e)–(f), the result would be Somigliana super-dislocations at the end.

(b). The rotation is in the (x, z) plane. It corresponds to a twist PD if terminated or if the ends are accommodated. The edge glide PD is shown in Fig. 6(c). The latter two can superpose to provide a mixed glide disclination, and for both the dislocations must satisfy the continuity axiom.

The remaining disclinations can also correspond to dislocation arrays [40], but that application is not unique. They also must satisfy continuity. If in-plane, their termini are partitioned, symmetric, Somiglinana disclination loops [41-44]. Fig. 6(d) is a skew-wedge disclination. The skew-wedge disclination has orthogonal wedge disclinations, but they can interact to form an equivalent, single wedge disclination with inclined to x and y and larger D vectors. In [37], this defect was called prismatic because half of a loop is the same as that of a prismatic super-dislocation (B normal to the plane of the loop). However, the present terminology seems more relevant. Fig. 6(e) shows the spin PD with orthogonal twist disclinations, formed from screw dislocation arrays. This PD could have rotated lines with mixed dislocations [30]. In the limit, there could be orthogonal edge dislocations with opposite signs The screw arrays would have minimum energy. Fig. 6(f) is a coherency/misfit PD, with two sets of dislocations. With Bilby dislocations, the PD corresponds to a coherent interface such as a type-I twin boundary or the fault in an extended dislocation. With discrete dislocations, the defect corresponds to a misfit PD, relieving coherency strains in two orthogonal directions.

# 3.3. Circular and other curved PDs

In the Green's function approach, the integrals can be written for the displacement field of an arbitrary curved or piece-wise straight dislocation in a plane [17]. However, they cannot be analytically solved except for special shapes such as circles, squares, etc. The fields of circular ring dislocations have been derived [45,46]. These can be used as Green's functions for some circular disclinations. Of the PDs in Fig. 6, the spin and coherency PDs can be represented as arrays of ring dislocations with Somigliana vectors s, analogous to Burgers vectors for standard dislocations, and PD vectors  $\Sigma$  replacing D as show in Fig. 7. The other Ds in Fig. 6 cannot be meaningfully represented by ring dislocation arrays. Ring dislocations are circular loops with s pointing in the radial direction [45,46]. The Somigliana solutions are closed, and no added defects are needed to satisfy continuity at the periphery. For the spin PD of Fig. 7(a), the  $\Sigma$  and  $\omega$  vectors are uniform but  $\Sigma$  is tangent to the line and  $\omega$  is normal to the loop. The ring dislocations have tangent vectors s: they are screw Somigliana ring dislocations [37,41-44]. The

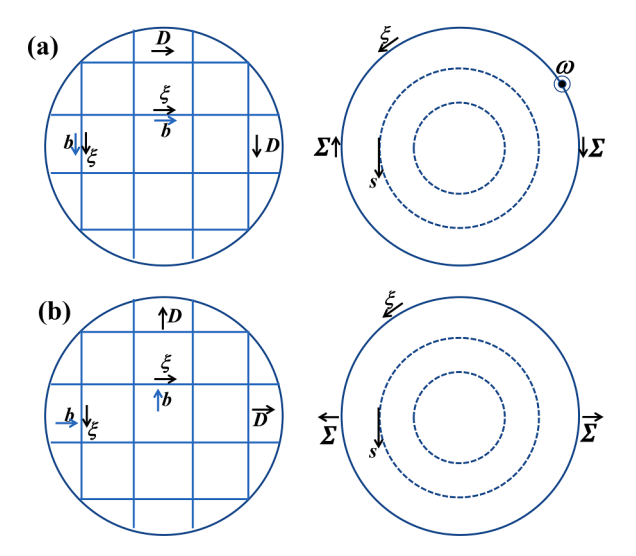


**Fig. 7.** The prismatic, spin and coherency PDs in Fig. 5. The figures on the right are the ring Somigliana PD equivalents of the arrays on the left.

Somigliana coherency disclination in Fig. 7(b) has  ${\bf D}$  and  ${\bf \omega}$  vectors that also vary in magnitude as a function of  ${\bf \theta}$ , from a maximum at  ${\bf \theta}=0$  to zero at  ${\bf \theta}=\pi/2$ , then to a minimum at  ${\bf \theta}=\pi$  and then an increase back to a maximum at  ${\bf \theta}=0$ . There is no ring equivalent for this case. For the coherency disclination, the  ${\bf \Sigma}$  and  ${\bf s}$  vectors point in a radial direction and  ${\bf \omega}$  is zero to linear order. There can be weak nonlinear rotations near the singularity.

Except for simple configurations like ring dislocations or ring disclinations, there are no analytical solutions for the fields. Curved interfaces of arbitrary shape are also Somigliana disclinations and Somigliana super-dislocations [37,41-44], often mixed in type. There is an integral for curved dislocations [12].

$$\frac{\partial u_m(\mathbf{r})}{\partial x_s} = b_i c_{ijkl} \int \frac{\partial^2 u_{mk}(R)}{\partial x_s' \partial x_l'} dA_j$$
(8)

As reviewed in [46] this leads to line integral expressions for curved dislocations. In turn these lead to line integrals of piecewise straight segments of dislocations. The extension has not been accomplished, but the equivalent for Somigliana dislocations is similar but with  $b_i$  replaced by the variable Somigliana vector  $s_i$  which is moved to the kernel.

$$\frac{\partial u_m(\mathbf{r})}{\partial x_s} = c_{ijkl} \int_{A} \frac{\partial^2 u_{mk}(R)}{\partial x_s' \partial x_l'} s_i dA_j \tag{9}$$

Here A is normal to an area element on a closed, curved area terminating at a curved dislocation loop, R = r' - r, r' is a vector from the origin to a point on the loop, and r is a vector from the origin to an arbitrary field point. The vector s is a function of r' for a circular loop or a loop of any shape. Eq. [8] is useful in numerical computation methods, so-called discrete dislocation dynamics, in turn useful for arrays of dislocations for a PD. Similarly, Eq. [9] could be useful for arrays of Somigliana dislocations and for curved PDs.

# 3.4. The stress and self-energy of PDs

The form of the stress field of a PD is exemplified by the result for a discontinuous tilt wall in Eqs. (21)–(54) in [14], and by the treatment of an extended core in [47], exactly equivalent to that for a PD. The complete stress field for a wedge PD, given in [3], can also be determined for a discontinuous tilt wall [14]. For example, the stress  $\sigma_{yy}$  to the right of a wedge ED and on the same plane is

$$\sigma_{yy} = -\frac{\mu D}{4\pi (1-\nu)L} \left[ \frac{r^2}{r^2 + (2L)^2} + \frac{1}{2} ln \frac{r+2L}{r} \right]$$

$$\cong -\frac{\mu D}{4\pi(1-\nu)L} \left[ \frac{L}{r} + \frac{L^2}{r^2} \right], r \to L$$
 (10)

$$\cong -rac{\mu B}{2\pi(1-
u)r}, \ r>> L$$

This form holds for all stress components in all directions. Eventually, at large r, the dependence assumes the super-dislocation form  $\sigma \propto 1/r$ . For the tilt wall case, the Burgers vector of the tilt dislocations is  $\boldsymbol{b}$ , and  $\boldsymbol{n}$  is the number of them in the length L. Aside from a constant core term, the total elastic energy (elastic contribution to the free energy) of a wedge PD, per unit length of line, is the same as that for an edge dislocation with a standard core of width L [47].

$$W_e = \frac{\mu B^2}{4\pi (1-\nu)} ln \frac{R}{L} \tag{11}$$

Here, R is the outer cutoff for the elastic field. The field within L varies and is not that of a super-dislocation. There are two cases of interest. With n constant, D = B is constant, and the  $W_e$  decreases logarithmically with increasing L With the density of dislocations n /L constant,  $D \propto L$ , and  $W_e$  increases with increasing L. The presence of

the  $(L/r)^2$  term in Eq. (10) raises an issue. The use of the SM and the associated linear elasticity means that  $(1/r)^2$ , second-order, terms in stress are neglected if (1/r) terms are also present. Such  $(1/r)^2$  terms are physically present because dislocations have two-dimensional dilatation fields and disclinations have rotational fields, both with displacements  $\propto (1/r)$  and shear stresses  $\propto (1/r^2)$ . There are similar line force fields in some cases. Thus, there is an issue as to whether the magnitude of the  $(L/r)^2$  terms is sufficient for them to be consistently included in SM results without following a fully nonlinear elastic model [48]. Solutions for  $W_e$  and the stress fields in the literature differ slightly [14]. This difference is associated with different assumptions for core fields. Thus, in comparing results one must use consistent core descriptions [13,49].

Correspondingly, the total thermodynamic force per unit line length on a partial in a PD is

$$F_T = \pm \Gamma + \int_{-L}^{L} (\boldsymbol{\sigma} \cdot d\boldsymbol{b} \times \boldsymbol{\xi}) dx = \pm \Gamma + \boldsymbol{F}$$
 (12)

Here, F is the elastic interaction force,  $\Gamma$  is the line tension associated with  $\Gamma$ , the interfacial free energy per unit area, excluding elastic contributions.  $\Gamma$  always points toward the fault. Also,  $d\mathbf{b}$  is the dislocation density between x and x+dx. For the discrete case the integral is replaced by the sum over n of  $(\sigma \bullet n\mathbf{b} \times \xi)$ . The stress  $\sigma$  is the sum of any term in the applied stress  $\sigma_a$ , the interaction stress  $\sigma_i$ , or, for the special case of a partial disclination, the self-stress  $\sigma_s$ . The long-range interaction force between PDs is  $\bullet B \times \xi$ , replacing the integral in Eq. (12). The stress  $\sigma$  varies with x for the short-range interaction. For the self-stress, the extension force at either end is

$$\mathbf{F} = (dW_e/dL)\mathbf{i} \tag{13}$$

This is a Peach-Koehler thermodynamic force, equivalent to a J integral, and is opposite in sign at either end where dL is opposite in sign. This emphasizes that the origin must be at the symmetric center of the PD. In contrast, a dissociated dislocation also has a fault, the stacking fault, but it is different in nature than for a PD. Eq. (12) applies, but there is no Bilby disclination content to the dissociated defect, and only surface energy in  $\Gamma$ , no core terms.

The spreading of a PD corresponding to the constant  $\boldsymbol{D}$  case entails a decrease in n/L, or equivalently, an increase in the dislocation spacing, d. The spreading is thermodynamically favored by the decrease in elastic strain energy (elastic free energy). The fault, while contributing only the rotation component of the distortion, has a surface energy associated with non-linear strain contributions from the core region and Gibbsian chemical terms arising from the symmetry breaking at the interface. Thus, analogous to the dislocation case, while the partials initially repel and move apart, there can be an equilibrium separation  $L_0$  in an unstressed body where the strain energy term is offset by the increased total surface energy, given by the condition,

$$F = \mp \Gamma \tag{14}$$

For the dissociated dislocation case, the extended dislocations are mixed, and the dominant edge or screw component follows the same rule.

Physically, in many applications, e.g., for disc-shaped precipitates or certain composite phases, an PD is pinned at the ends and cannot extend and the same is true for a PD spanning a grain. For wedge PDs, extension requires dislocation climb and is suppressed at low temperatures. A rare equivalent possibility is the emission of a pair of slant dislocations with slant Burgers vectors whose sum is parallel to the tilt Burgers vector. In contrast, coherency or glide PDs are glissile, and are free to move until they encounter an obstacle. For the constant n/L case, Eq. (12) shows that the energy increases with increasing L.

A different situation arises when the length changes because of the addition of a lattice dislocation, perhaps by the emissary dislocation mechanism [49],  $W_e$  increases, but the energy per dislocation decreases.

Essentially because the partials move apart. However, a lattice dislocation is removed so the total elastic energy of the system,  $\Delta W$ , decreases:

$$\Delta W = \frac{\mu b^2}{4\pi (1 - \nu)} \left( ln \left( \frac{R}{L} \right) - ln \left( \frac{R}{r_0} \right) \right) \tag{15}$$

partial from A at B. Thus, after relaxation, there are no elastic strains,  $\Omega=0$ , and the rotation  $\omega$  is the same for both arms. Thus, the continuity role of  $\omega$  extends to nonlinear arrays such as junctions and curved sections. The following axiom holds for either linear junctions or slant junctions.

The crystallographic rotation is the same at a junction between two PDs if the continuity vector  $\boldsymbol{\omega}$  is the same.

(16)

Hence, like the preceding case, there is a tendency for L to increase until pinned at the ends as discussed above. This is consistent with the recovery that takes place in stage I of work hardening. In stage I, dislocation mats tend to polygonize and form cells bounded by lowangle tilt walls.

#### 3.5. Extended disclinations junctions

An example of the many nonlinear arrays of ODs is a slant junction, exemplified by an L junction. The elastic strains of a single PD can be relaxed by lattice super-dislocations at the ends as in Fig. 8(a). For the loops in Fig. 4, these would be super-Somigliana dislocations. Junctions between two slant PDs are stress-free [14,25,35] provided that the  $\omega$ vectors of the two arms are the same and  $\Delta p = 0$ . The matrix and twin can be rigidly shifted by p, changing only shuffle vectors. However, if there is a difference  $\Delta p$  in the two vectors, a junction dislocation  $b = \Delta p$ is present. Thus, there is zero stress for two infinite arms or for two PDs of the same length, the same b, and the same p. An example is the Ljunction in Fig. 8(b), formed from two orthogonal PDs and with p = 0. This junction has no dislocation content. Fault A is a type I twin interface, while fault B is a PD that has been relaxed by lattice dislocations in the emissary dislocation mechanism [47]. In a second example, fault A in Fig. 8(c) is a tilt wall, initially a PD with an incompatibility strain field. The superposed partial at B annihilates the strain field of the

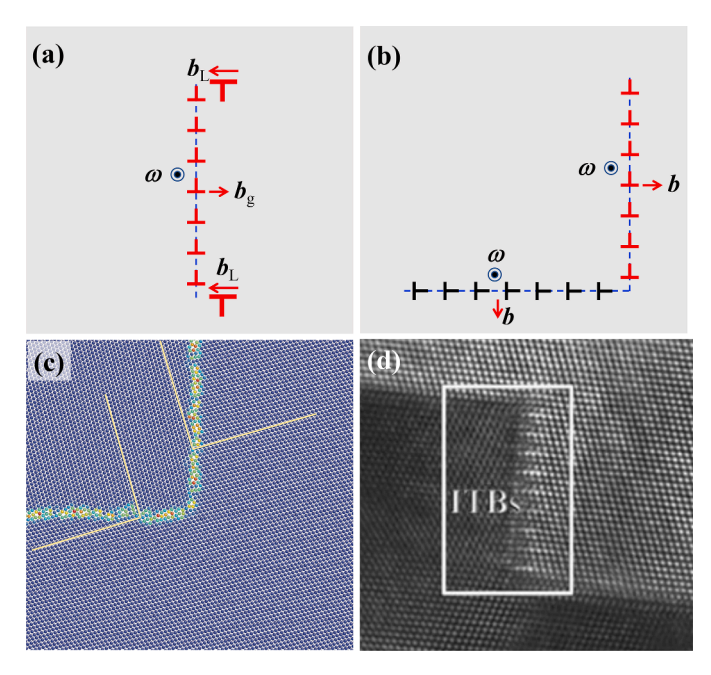


**Fig. 8.** (a) L junction where the elastic strains of a single PD can be relaxed by lattice dislocations at the ends. (b) A stress-free L junction with two PDs. (c) A stress-free L junction with the same  $\omega$ , showing no strains at a junction of two tilt walls. (d) HRTEM image of an L junction composed of a (111) coherent twin boundary and a {112} incoherent twin boundary [23].

When  $\omega = \Omega$ , there is no stress at the junctions. When  $\omega \neq \Omega$ , the difference represents an extrinsic, stressed PD. This agrees with the cut-and-paste notion of Frank as well as extending to the anisotropic elastic case [34].

The PD at B in principle could be on any plane for which  $\xi$  is a zone axis, but practically the choices are limited by symmetry [51–53]. An example of a relaxed L junction in a fcc crystal is a type I twin PD on (111) joining an orthogonal PD on the type II plane (11 $\overline{2}$ ), as shown in Fig. 8(d). The recovery mechanism and resulting relaxed interfaces can occur with different fault structures for the same ED. There are two variants for the type II (11 $\overline{2}$ ) plane, one with a repeated array of successive partial dislocations  $A\delta$ ,  $B\delta$ ,  $C\delta$  and the other with  $A\delta$ ,  $A\delta$ ,  $2\delta A$ . The former array is stable while the latter is metastable. Motion of pure  $h=3h_0$  steps has been observed in dynamic HRTEM [23]. There is no Peach-Koehler force for such motion, but there are second-order forces. The  $A\delta$ ,  $B\delta$ ,  $C\delta$  sequence provides a structural model for the 9R interlayer phase observed for (110) twin boundaries in copper [54,55,56]. There are other possible arrays, but they are all unstable.

All observed equilibrium multi-junctions of twins and grain boundaries entail superposed PDs. If multiple grain boundaries meet at a junction line, e.g., a triple grain boundary junction, the condition that the junction is free of long-range elastic strains is that the sum of the  $\omega$  vectors is zero, modulo  $2\pi$ , for the partial disclinations meeting at the line, provided that all sense vectors  $\xi$  point away from or toward the line. Since the junction is stress free, the force in Eq. (12) reduces the surface tension  $\Gamma$ . Thus, the sum of the line tensions  $\Gamma$  must also be zero. This leads to the well-known dihedral angle relation, which for a three-fold junction is

$$\frac{\Gamma_1}{\sin\omega_1} = \frac{\Gamma_2}{\sin\omega_2} = \frac{\Gamma_3}{\sin\omega_3} \tag{17}$$

Near the junction deviations can occur. For low-angle grain boundaries, there could be pileup formation near the junction line, as observed in Fig. 9(a). Also, if the surface energy varies with angle, or anisotropic elasticity is applied, there can be local torques at the junction, so that the boundaries are twisted locally.

One twin example is the classical 5-fold twin junction found in fcc crystals, as shown in Fig. 9(b). All partials have the same crystal symmetry, so the angles between faults should be equal. In addition to the rotations of the twin boundaries, each a  $70.32^{\circ}$  intrinsic wedge partial disclination, there remains a net angular misfit of  $7.35^{\circ}$ . Hence, in addition to the PDs satisfying Eq. (17), there are 5 superposed  $1.47^{\circ}$  wedge partial disclinations with the same  $\omega$ . Fig. 9(c) is a simulation of such a 5-fold set in Cu, with a free-surface boundary condition. All partials have the same crystal symmetry, so some of the non-linearities mentioned for grain boundaries are absent. However, there are nonlinear strains near the junction line, probably associated with a weak tendency for dislocation pileup formation. The leading term in such a case would be a dilatational field with strains  $\epsilon_{rr} = -\epsilon_{\theta\theta}$ , in agreement with Fig. 9(c).

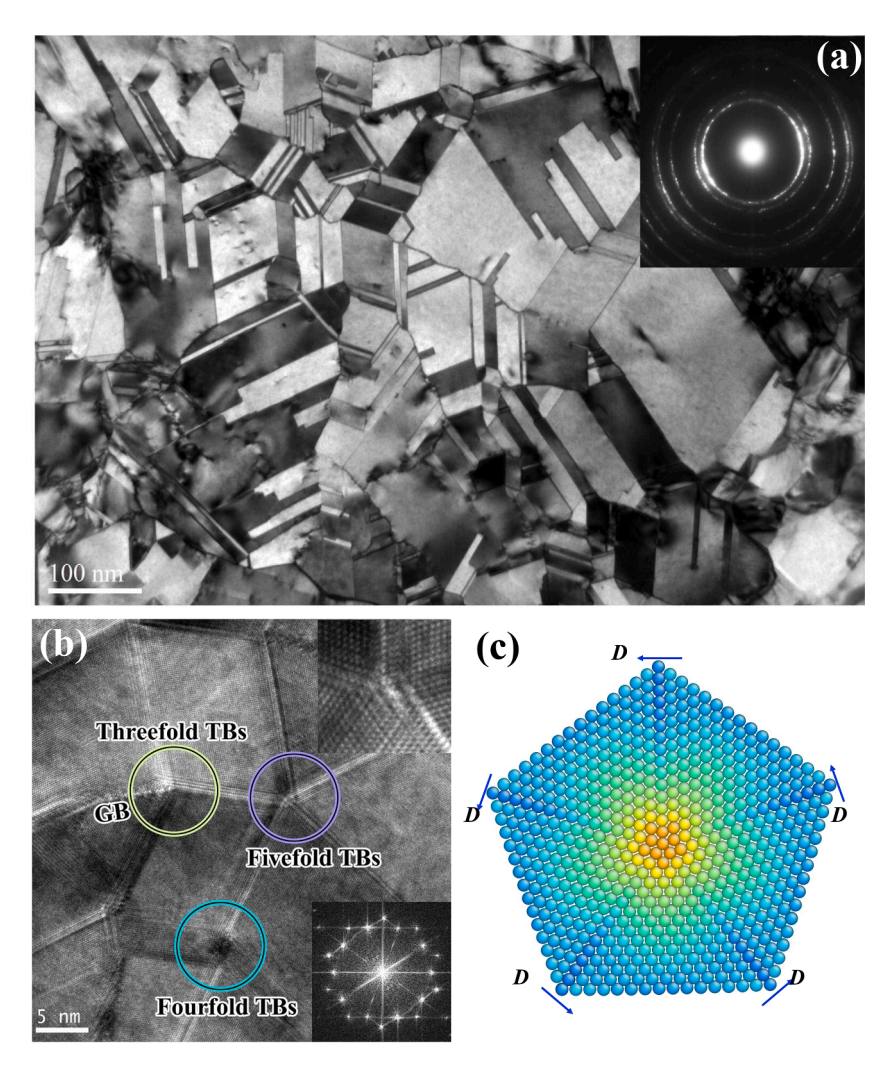


**Fig. 9.** (a) A bright-field TEM image showing multiple twins, low angle GBs and their junctions in a Ni sample synthesized by DC electrodeposition. (b) A bright-field TEM image showing multiple-fold twin boundaries [55]. The fivefold TBs are broadened to accommodate the mismatch angle as shown in the HRTEM image (inset). (c) Simulation of a 5-fold twin in *fcc* Cu [15], viewed along [110]. Differing colors indicate the magnitude of the hoop stress,  $\sigma_{\theta\theta}$ .

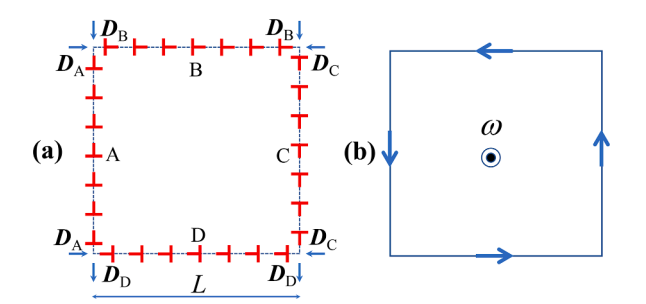


**Fig. 10.** (a). Fault quadrupole formed from four wedge PDs. (b) Net  $\omega$  vectors of (a) showing that there are no stresses.

## 3.6. Extended disclinations multipoles

There are two arrays of four PDs that comprise a fault quadrupole, important for disconnections, that have no long-range distortion component. The absence of long-range fields for polar arrays is the reason that there is a problem of scale dependence with the continuous dislocation model [57]. Contributions to the dislocation density are lost when the probe scale is large compared to multipole or dipole spacings.

Fig. 10(a) is composed of wedge or skew-wedge disclinations in a square/parallelogram arrangement with 90° junctions. Starting with a

square in a perfect crystal, one can imagine PDs A and C shearing the square to a rhombus and PDs B and D restoring the rhombus to a square. The rotation vectors  $\omega$  are the same for each PD as indicated in Fig. 10 (b). If the PDs are comprised of Bilby dislocations, there are no elastic strain fields. If the PDs are comprised of discrete dislocations with spacing d, there are elastic strains within a distance  $\sim d$  from the boundary. Twist PDs can exist as dipoles but are unlikely to exist as quadrupoles other than as components of the boundaries of a grain. An example is a fcc twin viewed along  $\lceil 1\overline{1}0 \rceil$  with  $\lceil 1\overline{1}1 \rceil$  planes.

The square in Fig. 11(a) is formed from four coherency or glide edge PDs. One can imagine PDs A and C converting the square to a rectangle and PDs B and D restoring the rectangle to a square. As depicted in Fig. 11(b), there is no continuity at the junctions and there is a strain quadrupole with no rotation. The field is limited to a distance  $\sim L$ . Fig. 11 (c, d) illustrates such a strain quadrupole in Mg, corresponding to a twin nucleus with  $P_M/B_T$  and  $B_M/P_T$ , where P designates the prism plane and P the basal plane [58]. The nucleus is identical to a quadrupole like that in Fig. 11(a), but with coherent boundaries. These boundaries appear in deformed hcp crystals, including steps of multiple height TDs [59]. The basal and prism planes are closely matched. The nucleus has coherent interfaces to reduce the total surface energy as is typical for nucleation. Processes. There are no misfit dislocations, and the nucleus has formed by a purely shuffle mechanism [54]. The nucleus grows by TDs with Burgers vectors P0. Eventually misfit dislocations form by the emissary

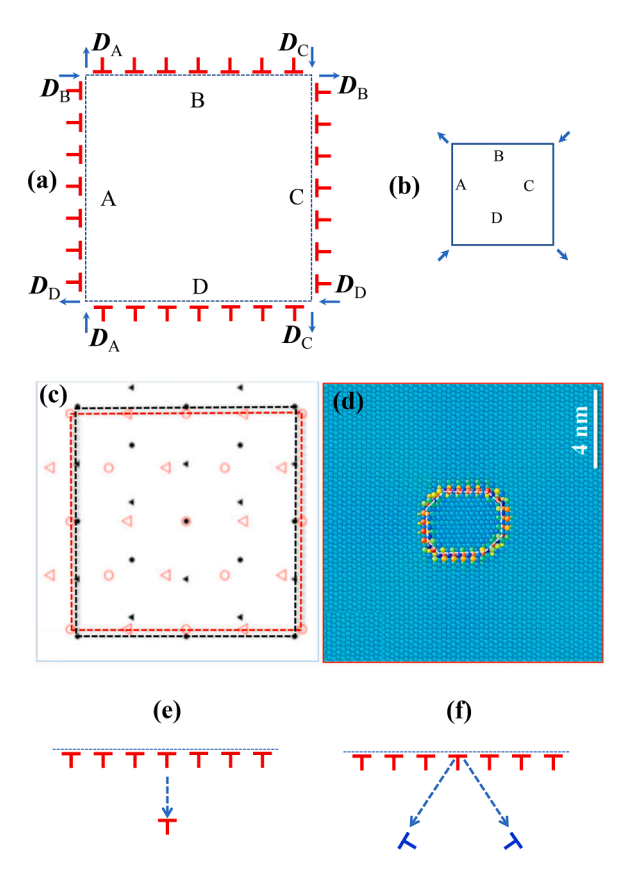


**Fig. 11.** (a) quadrupole of four coherency PDs. (b) Net D vectors. (c). Dichromatic pattern showing that there is coherency disregistry. (d). Simulated coherent nucleus with observable strains. (e). Displacement of misfit dislocation by climb as a TD shifts the interface. (f). Alternate shift by dissociation of a misfit dislocation into paired glide dislocations.

mechanism, most likely moving into the twin. Once misfit dislocations are present, the passage of a TD must be accompanied by the displacement of the misfit dislocation. One possibility is dislocation climb as in Fig. 11(e), but this can only occur at high temperatures and with perfect dislocations. At low temperatures the mechanism is that shown in Fig. 11(f), analogous to that for deformation of nanolayer structures [60, 61] and in oxidation reactions [62]. The misfit dislocation dissociates into a pair of glide dislocations.

If the dislocations in Fig. 11(a) are perfect, there are no coherency strains. For the case where the dislocation spacing is an atomic spacing, PDs *A* and *C* remove an atom and PDs *B* and *D* restore it. The strains then are removed, and the quadrupole is a null defect, simply representing a perfect crystal.

### 4. Twinning/transformation disconnections (TDs)

# 4.1. Twinning disconnections

The formation of a TD at a twin boundary is illustrated in Fig. 12(a) and (b). Once formed the Burgers vectors are determined by the difference of t vectors in Eq. (1). Because of the limitation on disclination lengths in hard crystals, one of their most prevalent appearances is at multiple height disconnections. Fig. 12(c) and (d) summarize the characteristics of a TD on a twin boundary: a Burgers vector and a step height  $h = mh_0$ , with m an integer and  $h_0$  the height of a unit disconnection. The TDs have both a structural role and a role as transformation or twinning defects. As a TD traverses a glide plane, the dislocation or disclination component shears a crystal, while the step component shifts the interface by h normal to the glide plane. The result is that a matrix plane becomes a twin plane. The equivalent for phase transformations is shown in Fig. 12(e). For this case, the lattice spacing normal to the glide plane also changes. This spontaneous change in length can be viewed as a set of spacing defects [28], and is represented by a dislocation component normal to the glide plane  $b_n$ . This shift requires no climb so the  $b_n$  component moves conservatively. The step motion produces a pure rotation as discussed below and is also accompanied by the shuffles required to complete the transformation. The shuffle analysis is simplified if one describes each atomic motif as a structural group [63] with an integer j of atoms: e.g., a dipole A–B with j=2. There are many possible sets of b and h for given dichromatic pattern [14]. The pair selected is a balance between a small b to minimize elastic self-energy and a small *h* to minimize shuffles.

Li [24] long ago showed that the displacement field of a disclination was equivalent to that of a pair of partials in a PD. Both descriptions have been used in describing disconnections as reviewed in [9,14]. In the small n limit, the arrangement would be a single dislocation. However, the disconnection description is superfluous for unit disconnections. Hence the disclination pair designation has never been used in dislocation theory [14,25,65,66]. The same is true for m=2, as exemplified for a partial dislocation bounding an extrinsic fault [14]. For some multiple height, as for a disconnection, the dislocation component transitions to a disclination. The issue is at what distance this occurs. The

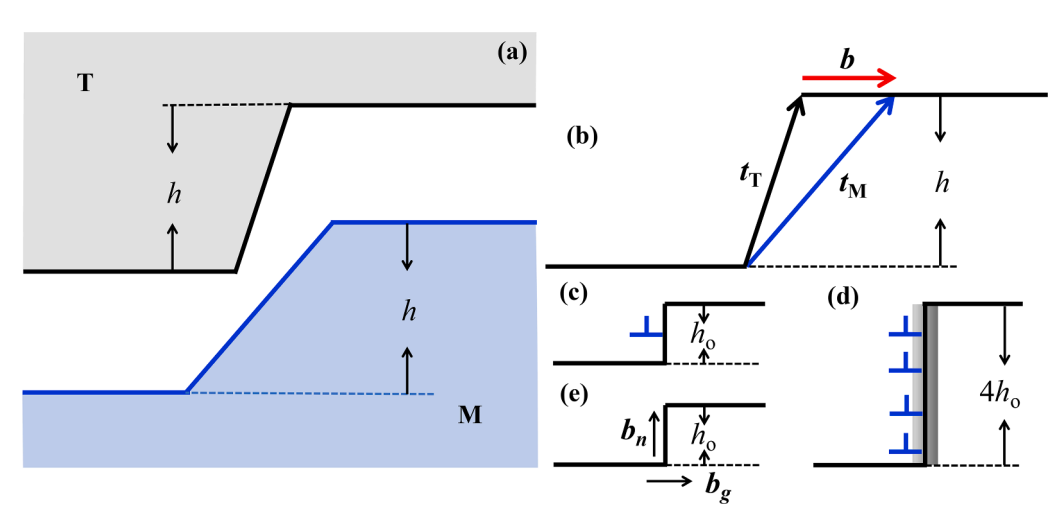


**Fig. 12.** (a) Two crystals containing short surface steps are joined, creating a TD with Burgers vector **b** and step height **h**. Two terrace interfaces are created on either side of the defect. If **h** is large, a disclination with vector **D** is created. (b). Definition of the Burgers vector **b** or the disclination vector **D**, and step height **h**. (c) Unit twinning TD with dislocation content. (d) Twinning TD with disclination content. (e). Unit TD for a phase transformation.

suggestion in [11] was that the disconnection component be described as a dislocation if the transition distance were within the nonlinear core region and a disclination if it were outside the core. Results for disclination fields indicate that the transition occurs for m=3 to 4. Hence, Li's description must be used when m is greater than this transition length, but it does not apply for smaller m, and never for unit disclinations. Neither model is exact in the core region. Atomistic simulations reveal local nonlinear strains [67], rigid shifts by p [68,69], structural units in high-angle grain boundaries [70], and thin interphases in layer structures [71]. These are incorporated either in the line tension  $\Gamma$  in Eq. (13) or the core parameter  $r_0$  in Eq. (14). Solute or vacancy-interstitial adsorption atmospheres also cause strain gradients and non-linearity in the core region. The core region can extend for tens of nm for the solute case [72].

Some special effects are associated with multiple height TDs and those with *j* multiple atoms in the motif or structural group at a lattice site. While the TDs have the same discrete or Bilby Burgers vectors, the shuffles are more complex. More generally, the dislocation vectors can vary from layer to later within the TD. So-called zonal dislocations are of this type [73]. Secondly, for twins with irrational twinning directions such as  $(10\overline{1}1)$  twins in *hcp* crystals, multiple height TDs can entail successive dislocations with two different Burgers vectors [74,75]. Thirdly, synchro-shuffle can occur when j > 1. Suppose j = 2 with A and B sites for identical atoms. Then normal shuffles entail A-A shifts and B-B shifts. However, shuffle vectors can be greatly reduced in some cases, which would be favorable energetically, if a two atoms shuffle by changing site type:  $A \rightarrow B$  and  $B \rightarrow A$ . This process was originally called synchro-shear, but in the TM corresponds to synchro-shuffle since there is no associated shear in cited cases. True synchro-shear is very rare. Examples of synchro-shuffle include twins in sapphire [76],  $(10\overline{1}2)$ twinning in Zr [77], and phase transformations in Laves phases [78] and olivine [79]. If A and B are different elements, the resultant pseudo-structure contains anti-site defects. An example is twinning in albite [64].

# 4.2. Transformation disconnections

Shear-shuffle phase transformations can be diffusional or martens-

itic. The major difference between twinning and the transformations is the presence of a Burgers vector component  $b_n$  in the TD. This component is a virtual climb dislocation associated with the difference in interplanar spacing normal to the commensurate terrace plane. The associated displacements are spontaneous as a TD moves. No atoms are added or removed, so no climb is needed. The presence of the virtual climb dislocation creates a mixed glide/wedge PD. This provides an added Peach-Koehler force for the motion of a TD, with magnitude  $n\sigma b_n$ , where the stress is now the normal stress relative to the terrace.

Since the collapse of the lattice associated with the removal of  $b_n$  is spontaneous, there is a short-cut useful for transformations in low symmetry structures such as Pu [80]. One imposes a Crocker, affine transformation to the matrix to a structure where the difference in d-spacing of planes parallel to the interface is removed. The resultant transformation is more-simply analyzed as a twin. The resultant structure then undergoes a reverse affine transformation to return the d-spacing, yielding the true product structure. This process can be applied for other types of affine transformation such as the shear version in ZrO [81] and CaCo<sub>3</sub> [82].

Because the PD is mixed glide/wedge for the phase transformation, the interface is that shown in Fig. 13(a, b). The interface can be viewed as a twin plane with a superposed set of wedge PDs like the Crocker result. As for all wedge PDs, the rotation  $2\alpha'$  associated with  $b_n$  is equally partitioned between the two phases. The TDs also serve as misfit defects, unlike twinning TDs. For Fig. 13(c), the Burgers vector components parallel to the terrace plane,  $b_g$  are equal and opposite to the sum of the Bilby dislocations  $b_i$  on the terrace planes. Thus, the resultant long-range distortion field is a pure rotation, with local strains only within a distance  $\sim L$  from the interface. The process of growing the product phase is essentially the reverse of the faceting process. The true rotation  $2\Delta\theta$  differs from  $2\Delta\theta'$ . This result and the partition of the rotation represent the major differences between the TM and aspects of the phenomenological theory. Equations for  $\Delta\theta$  are given in [20,83,84], where  $\Delta\theta$  is designated as  $\alpha$ .

The analysis of macroscopic shapes is complicated by the misfit role of the TDs, discussed in detail in [84]. For the phase transformation version of the lenticular plate, if a TD on the right is a misfit defect, that on the left is an anti-misfit defect. Thus, there is a strong tendency for the

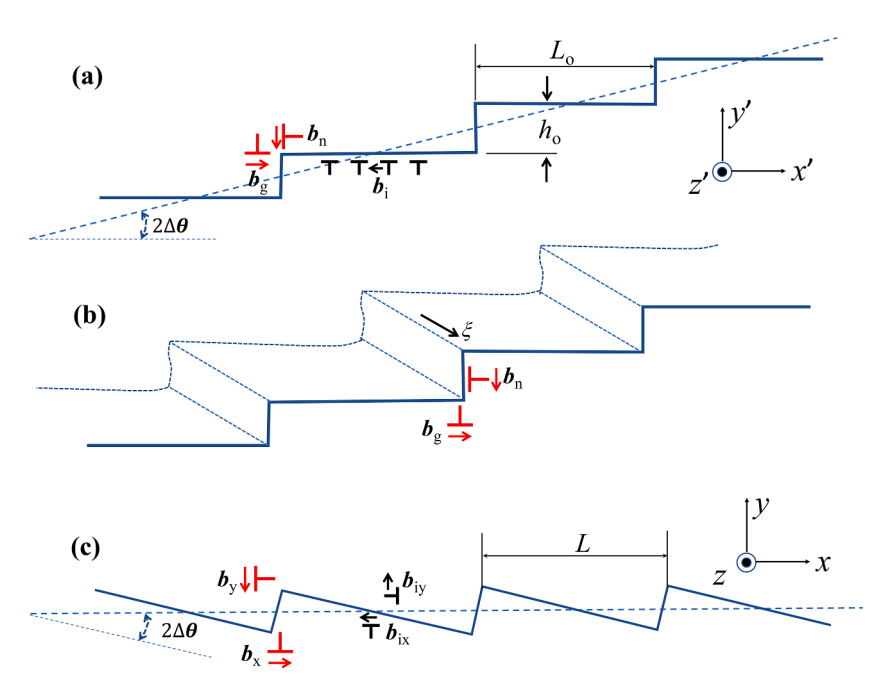


Fig. 13. (a). Section of a type I phase transformation with coherent interfaces as Bilby PDS and TDs as misfit defects. (b). 3D representation. (c) View relative to coordinates fixed on the mean interface (the habit plane). The Burgers vectors differ from those in (a) for these rotated coordinates. The angle  $2\Delta\theta$  corresponds to the orientation relationship.

shape to be asymmetrical. And, for a set of TDs like those on the right, evenly spaced TDs are favored energetically in misfit relief. Consequently, the shape of one side of the plate tends to have a triangular shape instead of a curved shape. Many triangular shapes are depicted in [85].

The phenomenological theory of martensitic transformations (PTMC) [86,87] is the classical treatment. The theory seeks a plane strain shear that produces an invariant plane, common to the matrix and product. The theory first envisioned that this plane is rational, with TDs moving on it. Bowles and Mackenzie [87] recognized that there was a problem matching the physical glide plane for TDs with such an invariant plane and introduced an empirical factor to account for the change in lattice spacing across low index planes. That factor qualitatively corresponds the normal component  $b_n$  in the TM. Later treatments explicitly showed that the invariant plane, while present, was irrational, agreeing with the TM. The later treatments [88-90] determined the structure of the irrational plane, analogous to the mechanisms for twinning. Micro-twins traversing the martensitic plates were added and explained the interface for (225) martensite plates in steel [88]. A model with microlayers of a second martensite variant traversing the main plate was added in [89]. In a sense, these mechanisms resemble the dual shear mechanism accompanying partitioning in the TM Yet, in some applications [91,92], it was envisioned that a simple shear mechanism with the rational shear plane an invariant plane was possible. Several efforts, culminating in [93], proved that such a simple mechanism was impossible. There is a parallel among the different descriptions. The primary simple shear is provided by TDs. The recovery is provided by lateral emissary lattice dislocations in the TM, micro-twins [88], or microlayers of a different variant [89]. We mention again the Crocker procedure described above that reduces the phase transformation analysis to that for a simple shear mechanism.

The above models for martensitic or diffusional phase transformations focus on type I/III mechanisms where the TDs glide on a  $k_1$  plane. Another possibility that has received less attention for phase transformations is that the TDs glide on  $k_2$  planes [11,83], particularly for the fast, near sonic velocity case. For the fast motion, there is a factor favoring a type II martensite mechanism compared to a type I mechanism. For a unit advance of a plate, a type I TD must move a larger distance,  $L_I$ , than for the type II twin,  $L_{II}$ . The required speed for the type II case is slower by the asperity ratio,  $L_{II}/L_{I}$ , and hence type II is favored [94]. The type II mechanism would also be favored in this manner by a preceding glide dislocation. The photon emission accompanying the dislocation motion is an energetic factor favoring the nucleation of a TD pair at the growing tip. The midrib observed in martensite plates in steel also suggests a type II mechanism.

# 5. Motion of TDs

As discussed in [20], the components of TDs have different consequences when a disconnection moves. A pure step or the step component of a disconnection, shown in Fig 14(a), produces only rotation with no linear strain field. The corners all resemble L junctions and there are no strain fields,  $\Omega = 0$ . As with the linear PDs treated previously, all terraces in a step can be considered as PDs comprised of Bilby dislocations. A step has the same  $\omega$  rotation vectors as the terrace. To separate these crystallographic PD components from those with strain fields, we represent them by an angle symbol. The dislocation or extrinsic PD component of a TD produces plastic shear or extension when it moves and elastic strain for a TD at rest. We represent these extrinsic components by arrays of dislocation symbols. Fig. 14(b) shows a multiple height PD and its step and extrinsic disclination components. Fig. 14(c) shows an analogous slant PD. Fig. 14(d) shows the relaxation of an PD into a pure step, e.g., by the emissary dislocation mechanism [51]. A pure slant step of any angle can be created in this manner. Fig. 14(e) shows an intrinsic curved step. There is no first-order strain field for the pure steps and the  $\omega$  vectors are continuous. There are second-order

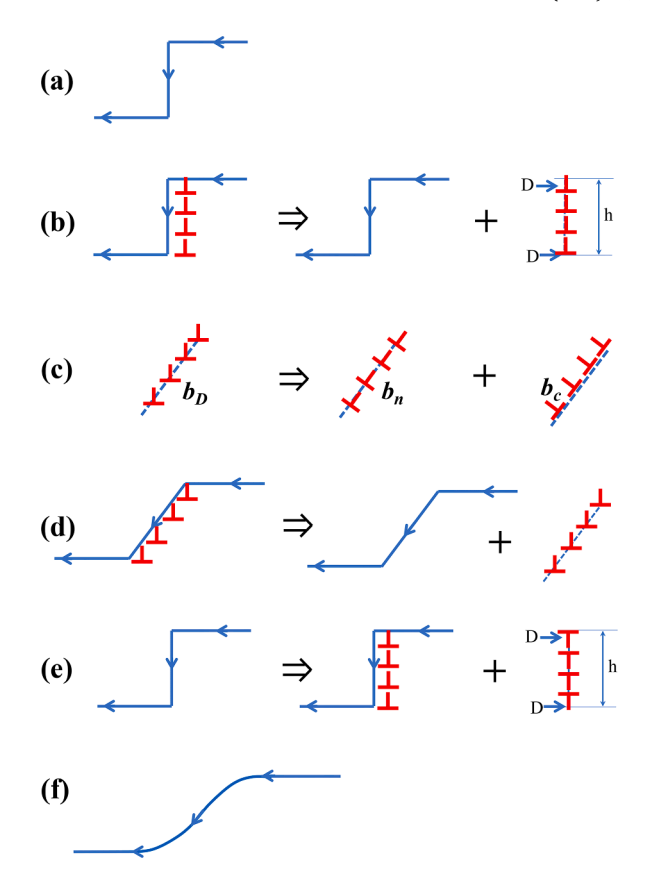


**Fig. 14.** (a) Step in twin with continuous  $\omega$  vector, (b) Disconnection composed of a pure step and a wedge PD. (c). Mixed PD composed of a wedge PD and a coherency PD. (d). Slanted disconnection composed of a pure step and a mixed wedge/coherency PD. (e). Disconnection with a curved step. (f). Curved pure step.

effects at corners [95]. The absence of first-order elastic strain for these intrinsic steps is consistent with Frank's formula for a general grain boundary [35]. There are examples where an intrinsic step relaxes to a slant step to reduce surface energy [15]. If this occurs without a change of the Bilby dislocation Burgers vector,  $b_D$  as in Fig. 14(f), the TD becomes extrinsic, with mixed character tilt,  $b_n$ , and coherency,  $b_c$  [15]. The coherency disclination component produces a strain field. These results extend in general to all junctions. L-junctions in NaCl [96] and Mo [97] are examples.

When unit TDs move, they tend to accumulate into larger steps [72–74]. This corresponds to the increase in step height of the multiple height disconnection by the continued addition of unit TDs. A single dislocation is attracted at short range and repelled at long range. As demonstrated by the calculations in [98], the distance from the PD at which the transition occurs increases monotonically with m. Thus, it becomes more favorable for a lattice dislocation to join an PD the greater is m. However, as suggested in [98,99], there is a value of m where further additions of TDs become unlikely. While the repulsive region becomes further from the PD with increasing m, the magnitude of the repulsive force increases with *m*, so it becomes more difficult for a lattice dislocation to the enter the attractive region. There is a likely maximum value of m in the range 10-15, and many observed PDs at twin boundaries agree with this expectation [55]. Of course, there are configurations other than TDs where longer lengths are possible. A similar situation arises at the blunt tips of deformation twins [100].

# 6. Recovery

A simple form of recovery is for dislocations with vectors  $-\mathbf{B}/2$  at

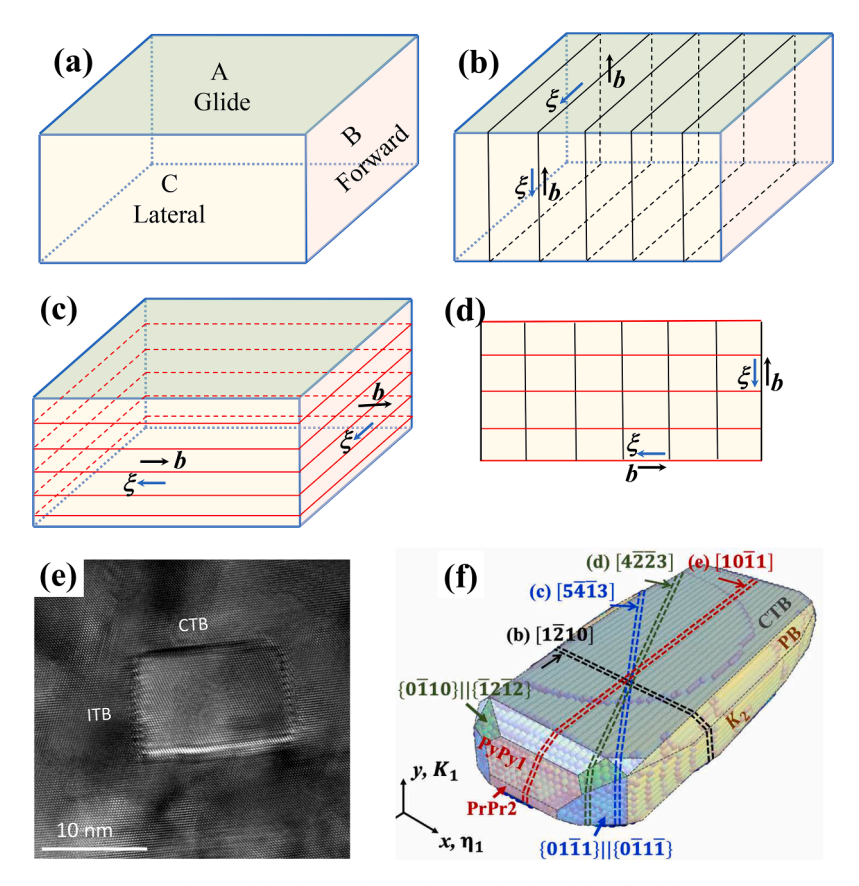


Fig. 15. (a) Recovered blocky type I twin. Face A is the TD glide plane and twin plane with edge-glide Bilby dislocations. Face B is the forward plane with edge Bilby dislocations. Face B is the lateral plane with a cross grid of screw-glide dislocations. (b) Bilby dislocations producing the twin rotation on face A and contributing screw components on face C are shown for the recovered twin. (c). Bilby dislocations on face A extending to face C. (d). A lattice dislocation on face A extending to face C, making  $\Omega = 0$ , and relaxing the interfaces. The total Bilby dislocations on face C form a twist boundary. (e). A HRTEM image of a recovered (111) twin in Al. (f). Atomistic simulations of  $a < 10\overline{12}$  twin nucleus showing multiple facets. PyPy1 and PrPr2 refer to  $(\overline{1101})_{M}||(0\overline{111})_{T}$  and  $(\overline{1210})_{M}||(1\overline{210})_{T}$ ; PB refers to  $(10\overline{10})||(100\overline{12})||(100\overline{12})$  is a bonded  $k_2$  interface [103].

each end of an RD to compensate the disclination vectors  $\mathbf{D}/2$  [9]. In many crystals these vectors cannot exactly compensate, but there is a best choice with a minimum difference. This corresponds to the near-coincidence model [101].

While the mechanistic focus in twinning theory is on the formation of twins, observations of twins are of recovered structures. We first consider the fully recovered blocky type I/III twin in Fig. 15(a). The analysis resembles that for junctions. The three surfaces are identified as the glide plane, the forward plane, and the lateral plane. Most analyses are two dimensional, with faces ABCD shown in a projection along the TD line direction. Recently, attention was drawn to the lateral interface [102,103]. Severe incompatibilities exist on the BD faces. Depicted in Fig. 15(b), the edge Bilby dislocations on face A extend as screws on face C. As shown in Fig. 15(c), the edge Bilby dislocations on face B extend as screws on face C. Together the Bilby screw dislocations produce a twist boundary on face C as shown in Fig. 15(d), so all faces have the same  $\omega$ . While maintaining the crystallographic rotation, the incompatibilities are removed by an array of lattice dislocations with spacing  $d_L$  so that  $\Omega \cong 0$  There are elastic strains only within a distance  $\sim d_L$ from the interface. The final description of the blocky twin is wedge PDs on faces A and B, and a spin PD on face C.

An example of a blocky recovered twin like that in Fig. 15(e), is a *fcc* twin with orthogonal planes A=(111),  $B=(\overline{11}2)$  and  $C=(\overline{11}0)$ . Another example is a recovered blocky  $(10\overline{1}2)$  twin in Mg [101], which is more complicated because the B face is irrational, and the C face is not a low index plane before relaxation. TEM characterizations and atomistic simulations in [102] revealed that the B face is relaxed into low energy interfaces comprising  $(\overline{1012})||(10\overline{12})|$  and  $(10\overline{10})||(0001)|$ , and

the C face is relaxed into low energy interfaces comprising  $(\overline{1}101)_M||(0\overline{1}11)_T$  and  $(\overline{1}2\overline{1}0)_M||\{1\overline{2}10\}_T$ , as shown in Fig. 15(f).

When a TD with disclination character increases in step height, its strain energy continually increases. The long-range strain can be recovered dynamically or statically by the emission of a lattice dislocation with a Burgers vector equal in sign to the dislocations in the TD. An opposite-signed lattice dislocation then resides in the TD, cancelling part or all the TD field. An example is a twin in Mg with the  $k_1$ , glide plane ( $\overline{1}012$ ), a glide vector  $b_g = 1/15 < 10\overline{1}1 >$ , a forward plane ( $\overline{1}01\overline{2}$ ), and a lateral plane  $(\overline{2}110)$  [101,102]. For Mg the cancellation by a lattice dislocation is not perfect but is a minimum at m = 14, as shown in Fig. 16 (a, b). The structure with m = 14 corresponds to the near O-lattice structure described in [101]. Observations of many HRTEM steps summarized in Fig. 16(c) reveal that the actual favored step height is m = 7. This indicates that the lattice disconnection with m = 14dissociates into two partial disconnections, demi-defects in the topological theory [50]. This observation agrees with the theoretical expectation. In a direct view of the lateral face, the resolution of screw dislocations is difficult, but the view normal to the forward face in Fig. 16(d) reveals the emergent points of the misfit screw dislocations.

There is another form of recovery for a type II twin. As described in [105,106], the twin boundary for a type II twin is irrational. Yet in many cases it is close to a low index plane. In such a case, driven by the reduction in surface energy, the interface of Fig. 17(a) breaks up into low index facets bounded by disclinations with Burgers vectors, see Fig. 17(b), nearly equal and opposite to the net Burgers vector of the Bilby dislocations in the facet. As reviewed in [103], there are several faceted structures for Type II/IV twins that agree precisely with the TM

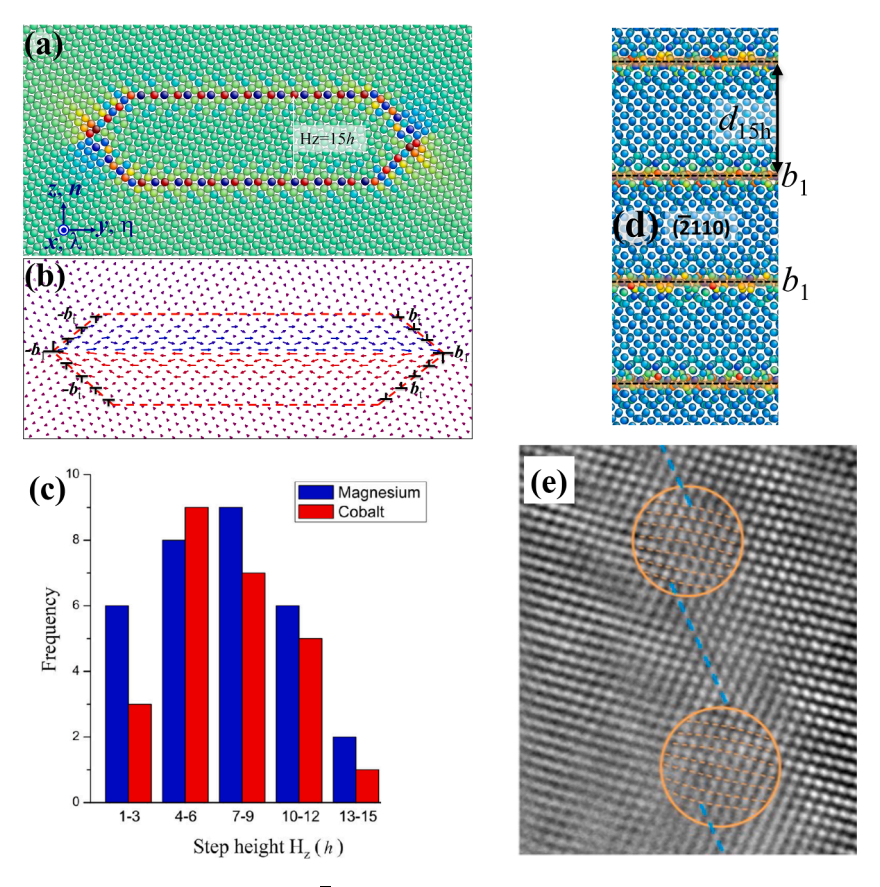


**Fig. 16.** (a). Simulation of the glide and forward planes for a  $(10\overline{1}2)$  type I twin in Mg after recovery. (b). Displacement plot showing the TD vectors  $b_g$  and a compensating lattice vector  $b_L$ . (c). Distribution of step heights measures in HRTEM. (d). View normal to the forward face showing the emergent points for the misfit screw lattice dislocations on the lateral face. (e). High-resolution TEM and corresponding fast-Fourier transform (FFT) patterns of the lateral interface composed of CTBs and misfit dislocations [101]. The blue dash line on a  $(10\overline{1}2)$  plane roughly indicates the possible boundary location.

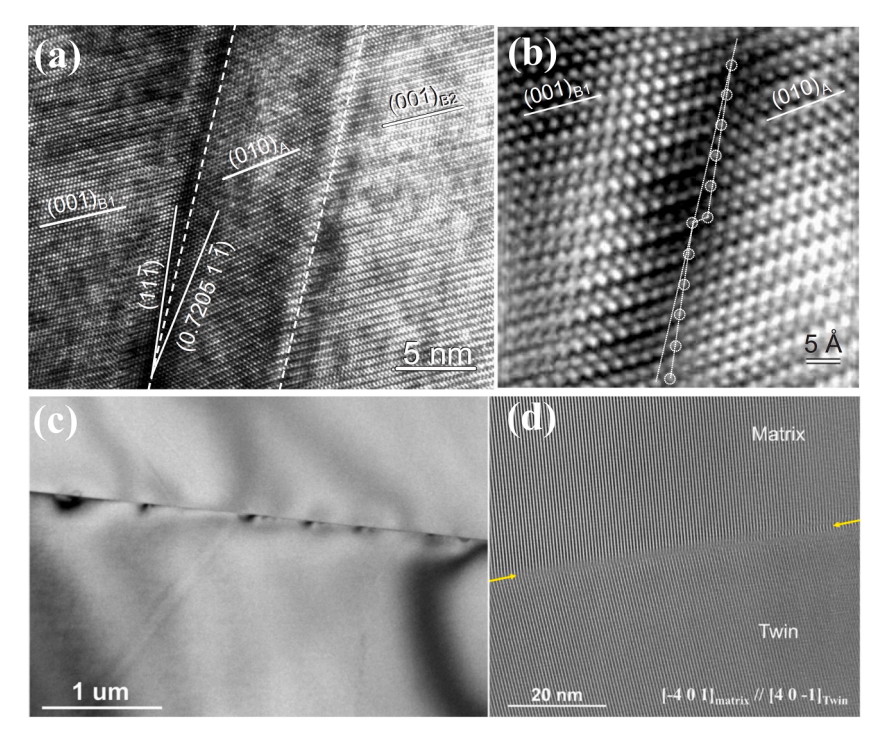


Fig. 17. (a) HRTEM micrograph of [011] type II twins in NiTi martensite with  $[101]_A$  ||  $[1110]_B$ . (b) IFFT HRTEM image of [011] type II twin boundaries between variants B1 and A [100,101]. (c) A bright field image of pericline twin in bytownite viewing along [401]. Twin boundary is faceted with  $\langle L_I \rangle = 550$  nm. (d) A HRTEM image of pericline twin boundary in bytownite containing a disconnection at the center [104].

predictions, as shown in Fig. 17(c) and (d).

The discussion here refers to emissary dislocations as the entities providing recovery. For the lenticular twins considered here, microtwins traversing the twin would be an alternative to emissary dislocations in providing recovery. An example is provided in the analysis of twins in uranium-niobium alloys [107].

#### 7. Discussion

As long known, the displacement field of an edge dislocation, while correct in the linear elastic approximation, contains a false, non-physical divergence in the y-direction [22]. This is reflected in a shift of origin and the presence of a non-zero  $\mathbf{M}$  integral [108]. The motion of this false line force implies work done by  $\sigma_{yy}$  stresses, which would alter the Peach-Koehler relation, for example. A recent emendation [39] corrects this by adding a true equal and opposite line force that cancels the false one and cancels  $\mathbf{M}$ . Thus, the only relevant plastic displacement is  $\mathbf{b}$ . The resultant stress fields are modified by factors ranging up to 20 % in the isotropic elastic approximation and this affects defect interactions. The only change here is to add the factor  $\eta$  to Eqs. (11) and (12).

$$\eta = \frac{2(2 - 3\nu + 2\nu^2)}{(3 - 2\nu)} \tag{18}$$

For example,  $\eta \cong 1.046$  when  $\nu = 1/3$ . However, the present work emphasizes structure and symmetry which are unaffected. The major nonlinear changes presented in this application are associated with symmetry requirements in the TM together with the accompanying selection of origin and partitioning of displacements.

There were many early associations of type I twin boundaries and wedge disclinations, extending to the present. The TM modifies these ideas by using embedded coordinates, adding geometrical nonlinearity, and emphasizing both the partial nature of the disclinations and partitioning. Moreover, partitioning causes type II twins to differ from the classical descriptions and leads to the new definitions of twin types in Appendix A. Added there are new types III and IV, extensions of I and II when the respective  $\chi_1$  and  $\chi_2$  twinning directions are irrational. The resultant twin boundaries are rotated significantly relative to the classical twins, although the new results are consistent with general twinning theory [109,110]. As reviewed in [111], the TDs were defined earlier as twinning dislocations. However, the focus was only on the Burgers vector, not the step character nor on the disclination character for larger step heights, both key features in the TM, where the combined defect is the twinning disconnection. Again, with linear elasticity, there was no consideration of partitioning, with its important relation to local rotations. Thus, the TM modifies both aspects of classical theory.

The TM modifications are consistent with the SM [14]. In the SM, the use of embedded coordinates is implied but not specified in the original topological theory [21]. This usage entails a geometrical nonlinearity. In linear elasticity, asymmetrical forms of displacements are invariably used in deriving the displacements for dislocations This procedure has no effect on the derived long-range stresses or strains, but there are asymmetries near the core. To obviate this, separate displacements are selected in the latest versions of the TM, consistent with the symmetry at the cut-plane.

For a screw dislocation, the displacement fields are:

$$u_z = \frac{b\theta}{2\pi} [-\pi/2 < \theta < \pi/2]$$
 (19)

$$u_z = -\frac{b\theta}{2\pi} [\pi / 2 < \theta < 3\pi / 2]$$

Similar results apply for edges. In the TM, the DP and DC are inherently embedded on lattice sites. Thus, symmetry is fulfilled automatically. The same is true for the TDs and PDs considered here, as well as lattice dislocations and perfect disclinations. These symmetrical forms are important, for example, in boundary conditions for atomistic

simulations. We emphasize the need for a symmetrical origin for the elastic field in all cases as requires in the TM and SM.

Rotational discontinuities produce strain-fields characterized by D. Unlike Burgers vectors for dislocations, these vectors do not sum for PDs and are supplanted by the continuity vector  $\omega$ . Hence, the non-intuitive result is that  $\omega$  vectors sum at a slant junction, but D vectors do not. The applications to blocky twins and recovered steps at TDs demonstrate this truism. The same concepts apply for shear-shuffle phase transformations, but the PDs and D vectors are mixed. As treated here, the TM readily explains the motion of simple tilt and twist grain boundaries by TDs. The TM applies for more general grain boundaries that can be considered as the superposition of multiple simple boundaries, but the applicable TD mechanism is diffusional, dominated by shuffles, including shear-type shuffles as treated in [14, Fig. 23.5].

We have clarified the historical nomenclature [43,44] in two senses. We showed that Li's description of a dislocation [24], a TD in the present context, as a disclination dipole, applies for TDs with steps of triple or more height, but not for unit TDs. Also, what were called dipoles are divided into dipoles and like-sign pairs. The PD or perfect disclination dipoles have equal and opposite strain fields and annihilate upon contact, analogous to other examples such as electron-hole pairs. The like sign pairs repel one another.

The steps or facets associated with deformation twins can be well described as PDs with a bounding fault in the hard crystalline materials. The faults consist of planar defects such as coherent and incoherent twin boundaries. An important observation is that these PDs may experience different kinetic barriers with respect to the direction of motion, i.e., directional asymmetry. Examples are twinning in hexagonal metals and {112} twinning in metals with a body center cubic structure. Correspondingly, these materials display strong plastic anisotropy. The present results can be incorporated into multiscale materials modeling and help develop the strategy of controlling twinning via tailoring the core structure of TDs.

We treat only hard materials here. Perfect disclinations are prevalent in soft materials but partial disclinations exist and can be described by the present results. Somigliana defects have been described for soft materials as well [112,113].

The focus here is on structure, although many TM/SM calculations follow the Green-function approach of Mura [12]. Recently, a significant, alternate, generalized theory has been developed [17,18]. As discussed, consistent with the usage established for fifty years of partial disclinations and faults, we prefer the designation PD to that of *generalized disclinations*, [17,18]. The theory provides an alternative to discrete dislocation dynamics theory and has the potential to determine fields for curved dislocation lines, PD faults, and Somigliana defects. An application of this theory to some of the concepts presented here, such as partitioning, would be valuable.

While not discussed here, we note that many of the same concepts would apply for double-ended microcracks.

# 8. Summary

- a) Previous linear elastic results are modified by the inclusion of embedded coordinates, a nonlinear geometry effect included in the topological model. The associated symmetry leads to equipartitioning of crystallographic displacements and a symmetrically placed origin.
- b) The standard model is applied for extended disclinations. The symmetry of plastic displacements is distinguished from crystal symmetry. The latter relates to a continuity vector that establishes the condition for pure rotation at a twin, grain, interphase interface.
- c) Disclinations and uniform dislocation arrays are equivalent except for nonlinear core terms. Differences in local stress fields in the general literature arise from different core models.

- d) Including curved defects, we identify six types of disclinations and relate them to curved dislocation arrays. Two of these can be described as arrays of Somigliana dislocations.
- e) Mechanisms are discussed for the recovery of disclination fields.
- f) Applications are presented for disconnections, lenticular and blocky twins, interface junctions, multipolar arrays, and shear-shuffle type phase transformations.

#### Declaration of competing interest

The authors declare that they have no known competing financial interests or personal relationships that could have appeared to influence the work reported in this paper.

# Acknowledgments

This work was financially supported by the US National Science Foundation (NSF) (CMMI- 2132336). We are pleased to acknowledge helpful discussions on this subject with A. Acharya, J.D. Embury, G. Hirth, R.G. Hoagland, T. Khraishi, T.E. Mitchell, F.R.N. Nabarro, J.F. Nie, R.C. Pond, C.N. Tomé, H. Zbib and W.-Z. Zhang.

#### Author statement

JPH and JW prepared the manuscript. JPH conceived this study. Both authors contributed to the research.

#### References

- V. Volterra, Sur l'équilibre des corps élastiques multiplement connexes, Ann. Ecole Normal. Super. 24 (1907) 401–517.
- [2] C. Somigliana, On the theory of elastic distortions, Rend. Accad. Lincei 23 (1914) 463–472.
- [3] R. deWit, The continuum theory of stationary disclinations, Solid State Phys. 10 (1960) 249–292.
- [4] G. Friedel, Les etats mesomorphe de la materié, Ann. Phys. 18 (1922) 273-274.
- [5] F.C. Frank, Crystal dislocations-elementary concepts and definitions, Phil. Mag. 42 (1951) 809–819.
- [6] F.R.N. Nabarro, Linear theory of static disclination, in: J.A. Simmons, R. deWit, R. Bullough (Eds.), Fundamental Aspects of Dislocation Theory, Nat.Bur. Stand., Gaithersburg MD, 1970, pp. 710–721.
- [7] J.D. Eshelby, The continuum theory of lattice defects, Solid State Phys. 3 (1956)
- [8] E. Kröner, K.H. Anthony, Dislocations and disclinations in material structures, Ann. Rev. Mater. Sci. 543 (1975) 43–72.
- [9] A.E. Romanov, V.I. Vladamirov, Disclinations in crystalline solids, in: F.R. N. Nabarro (Ed.), Dislocation in Solids 9, Elsevier, Amsterdam, 1992, pp. 191–422.
- [10] A.E. Romanov, A.L. Kolesnikova, Application of disclination concept to solid structures, Prog. Mater. Sci. 54 (2009) 740–769.
- [11] J.P. Hirth, G. Hirth, J. Wang, Disclinations and disconnections in minerals and metals, PNAS 117 (2009) 196–204.
- [12] T. Mura, Continuous distribution of moving dislocations, Phil. Mag. 8 (1968) 843–857.
- [13] R. deWit, Theory of disclinations. II. Continuous and discrete disclinations in anisotropic elasticity, J. Res. 77 (1973) 49–100.
- anisotropic elasticity, J. Res. 77 (1973) 49–100.
   P.M. Anderson, J.P. Hirth, J. Lothe, Theory of Dislocations, 3rd ed., Cambridge University Press, UK, 2017.
- [15] J.P. Hirth, J. Wang, C.N. Tomé, Disconnections and other defects associated with twin interfaces, Prog. Mater. Sci. 83 (2016) 417–471.
- [16] R. deWit, Partial disclinations, J. Phys. C Solid State Phys. 5 (1972) 529-538.
- [17] A. Acharya, C. Fressengeas, Continuum mechanics of the Interaction of phase boundaries and dislocations, Proc. Math. Stat. 137 (2015) 123–165.
- [18] C. Zhang, A. Acharya, On the relevance of generalized disclinations in defect mechanics, J. Mech. Phys. Sol. 119 (2018) 188–223.
- [19] B.A. Bilby, R. Bullough, E. Smith, Continuous distributions of dislocations: a new application of the methods of non-Riemannian geometry, Proc. Roy. Soc. (London) A231 (1955) 263–273.
- [20] J.P. Hirth, Pond R.C, R.G. Hoagland, X.Y. Liu, J. Wang, Interface defects, reference spaces and the Frank-Bilby equation, Prog. Mater. Sci. 58 (2013) 749–823
- [21] R.C. Pond, Line defects in interfaces, in: F.R.N. Nabarro (Ed.), Dislocations in Solids 8, North-Holland, Amsterdam, 1981, pp. 1–67.
- [22] J.P. Hirth, Dislocations, steps and disconnections at interfaces, J. Phys. Chem. Solids 55 (1994) 985–989.
- [23] N. Li, J. Wang, A. Misra, X. Zhang, J.Y. Huang, J.P. Hirth, Twinning dislocation multiplication at a coherent twin boundary, Acta Mater. 59 (2011) 5989–5996.

[24] J.C.M. Li, Disclination model of high angle grain boundaries, Surf. Sci. 31 (1972) 12–26.

- [25] F.R.N. Nabarro, Theory of Crystal Dislocations, Cambridge University Press, U.K., 1967.
- [26] R. deWit, Theory of disclinations. IV. Straight disclinations, J. Res. 77 (1973) 602–658.
- [27] J.P. Hirth, G. Hirth, J. Wang, Types III and IV deformation twins in minerals and metals, PNAS 119 (2022) e2118253119.
- [28] J.P. Hirth, R.C. Pond, J. Lothe, Spacing defects and disconnections in grain boundaries, Acta Mater. 55 (2007) 5428–5437.
- [29] J.D. Eshelby, The determination of the elastic field of an ellipsoidal inclusion and related problems, Proc. Roy. Soc. (London) 241A (1957) 306.
- [30] N.I. Muskhelishvili, Some Basic Problems of the Mathematical Theory of Elasticity, Noordhoff, Leyden, 1975.
- [31] D.M. Barnett, J. Lothe, An image force theorem for dislocations in anisotropic bicrystals, J. Phys. F 4 (1974) 1618–1635.
- [32] T.C.T. Ting, Anisotropic Elasticity, Oxford Univ. Press, UK, 1996.
- [33] J. Dundurs, Y. Mura, Interaction between an edge dislocation and a circular inclusion, J. Mech. Phys. Solids 12 (1964) 127–138.
- [34] J.P. Hirth, G.M. Barnett, J. Lothe, Stress fields of dislocation arrays at interfaces in bicrystals, Phil. Mag. 40A (1979) 39–47.
- [35] F.C. Frank, in: Report of the Symposium on the Plastic Deformation of Crystalline Solids, Carnegie Inst Tech, Pittsburgh Pa, 1950, pp. 150–161.
- [36] J.D. Eshelby, J.P. Hirth, R. deWit, Panel discussion, in: J.A. Simmons, R. deWit, R. Bullough (Eds.), Fundamental Aspects of Dislocation Theory, Eds 1, Nat. Bur. Stand., Washington, D.C., 1970, pp. 725–727. Spec. Publ. 317.
- [37] J.P. Hirth, R.W. Armstrong, Straight and curved disclinations and dislocation equivalents, Phil. Mag. 100 (2020) 25–37.
- [38] Y.T. Zhu, J. Narayan, J.P. Hirth, S. Mahajan, X.L. Wu, X.Z. Liao, Formation of single and multiple deformation twins in nanocrystalline fcc metals, Acta Mater. 57 (2009) 3763–3770.
- [39] J.P. Hirth, Modification of the elastic field of an edge dislocation, Phil. Mag. 103 (2023) 1992–1997.
- [40] J.P. Hirth, Stabilization of strained multilayers by thin films, J. Mater. Res. 8 (1993) 1572–1577.
- [41] A.E. Romanov, M. Hecker, Elastic fields of straight linear Somigliana dislocations near a free surface, phys. stat. sol. (a) 115 (1) (1989) K159–K162.
- [42] P. Müllner, A.E. Romanov, Internal twinning in deformation twinning, Acta Mater. 48 (2000) 2323–2337.
- [43] P. Müllner, A.E. Romanov, Modeling internal twinning with disclinations and Somigliana dislocations. Solid State Phenom. 87 (2002) 239–244.
- [44] A.L. Kolesnikova, A.E. Romanov, Virtual circular dislocation-disclination loop technique in boundary value problems in the theory of defects, J. Appl. Mech. 71 (2004) 409–417.
- [45] I. Demir, J.P. Hirth, H. Zbib, The Somigliana ring dislocation, J. Elast. 28 (1992) 223–246.
- [46] I. Demir, T.A. Khraishi, The torsional dislocation loop and mode III cylindrical crack, J. Mech. 21 (2005) 109–116.
- [47] J. Lothe, Dislocations in continuous elastic media, Mod. Probl. Condensed Mater. Sci. 31 (1992) 175–236.
- [48] C. Teodosiu, Non-linear effects in the elastic field of single dislocations, in: Elastic Models of Crystalline Defects, Springer, Berlin, 1982, pp. 207–264.
   [49] J. Lothe, J.P. Hirth, Dislocation core parameters, phys. stat sol. 242b (2005)
- 836–841.
- [50] A.W. Sleeswyk, Emissary dislocations: theory and experiments on  $\alpha$ -iron, Acta Mater. 10 (1962) 705–725.
- [51] R.C. Pond, D.S. Vlachavas, Bicrystallography, Proc. R. Soc. (London) 386A (1983) 95–143.
- [52] O.B.M. Hardouin Duparc, A review of some elements for the history of mechanical twinning centred on its German origins until Otto Mügge's K1 and K2 invariant plane notation, J. Mater. Sci. 52 (2017) 4182–4196.
- [53] D.Y. Xie, G. Hirth, J.P. Hirth, J. Wang, Defects in deformation twins in plagioclase, Phys. Chem. Min. 46 (2019) 959–975.
- [54] G.H. Campbell, D.K. Chan, D.L. Medlin, J.E. Angelo, C.B. Carter, Dynamic observation of the FCC to 9R shear transformation in a copper Σ=3 incoherent twin boundary, Scr. Mater. 35 (1996) 837–842.
- [55] C.B. Carter, D.L. Medlin, J.E. Angelo, M.J. Mills, The 112 lateral twin boundaries in FCC metals, Mater. Sci. Forum 207-209 (1995) 209–212.
- [56] J. Wang, O. Anderoglu, J.P. Hirth, A. Misra, X Zhang, Dislocation structures of Σ3 (112) twin boundaries in face centered cubic crystals, Appl. Phys. Lett 95 (2009) 021908.
- [57] E. Kröner, Benefits and shortcomings of the continuous theory of dislocations, Int. J. Solids Struct. 38 (2001) 115–1134.
- [58] M.Y. Gong, J.P. Hirth, Liu Y, Y. Shen Y, J. Wang, Interface structures and twinning mechanisms of twins in HCP metals, Mater. Res. Lett. 5 (2017) 449–464.
- [59] M.Y. Gong, H. Ma, K. Yang K, J.F.Nie Liu, J. Wang, Symmetric or asymmetric glide resistance to twinning disconnection? NPJ Comput. Mater. 8 (2022) 168.
- [60] J. Wang, S.K. Yadav, J.P. Hirth, C.N. Tomé, I.J. Beyerlein, Pure-shuffle nucleation of deformation twins in HCP metals, Mater. Res. Lett. A 1 (2013) 126–132.
- [61] A. Misra, J.P. Hirth, R.G. Hoagland, J.D. Embury, H. Kung, Dislocation mechanisms and symmetric slip in rolled nano-scale metallic layers, Acta Mater. 52 (2004) 2387–2394.
- [62] A. Misra, J.P. Hirth, R.G. Hoagland, Length-scale-dependent deformation mechanisms in incoherent metallic multilayered composites, Acta Mater. 53 (2005) 4817–4824.

- [63] A. Pieraggi, R.A. Rapp, Stress generation and vacancy annihilation during scale growth limited by cation-vacancy diffusion, Acta Metall. 36 (1988) 1281–1289.
- [64] J.P. Hirth, J. Wang, G. Hirth, A topological model for defects and interfaces in complex crystal structures, Am. Mineral. 104 (2019) 966–972.
- [65] J. Friedel, Dislocations, Addison-Wesley, Reading M.A., 1964.
- [66] W. Cai, W.D. Nix, Imperfections in Crystalline Solids, Cambridge Univ. Press, UK, 2016.
- [67] J. Wang, I.J. Beyerlein, Atomic structures of [0-110] symmetric tilt grain boundaries in hexagonal close-packed (hcp) crystals, Metall. Mater. Trans. A Phys. Metall. Mater. Sci. 43 (2012) 2569–3556.
- [68] A. Ostapovets, A. Serra, Review of non-classical features of deformation twinning in hcp metals and their description by disconnection mechanisms, Metals (Basel) 10 (2020) 1134–1154.
- [69] J.P. Hirth, J. Wang, C.N. Tomé, Disconnections and other defects associated with twin interfaces, Prog. Mater. Sci. 83 (2016) 417–471.
- [70] M.F. Ashby, F. Spaepen, S. Williams, The structure of grain boundaries described as the stacking of polyhedra, Acta Metall. 26 (1978) 1647–1663.
- [71] J.P. Hirth, Stabilization of strained multilayers by thin films, J. Mater. Res. 8
- [72] J.P. Hirth, D.M. Barnett, R.G. Hoagland, Solute atmospheres at dislocations, Acta Mater. 131 (2017) 20174–22019.
- [73] K. Kishida, M. Okutani, H. Inui, Direct observation of zonal dislocation in complex materials by atomic-resolution scanning transmission electron microscopy, Acta Mater. 228 (2022) 117756.
- [74] J. Wang, O. Anderoglu, J.P. Hirth, A. Misra, X. Zhang, Dislocation structures of Σ3 (112) twin boundaries in face centered cubic crystals, Appl. Phys. Lett. 95 (2009) 021908
- [75] J. Wang, I.J. Beyerlein, J.P. Hirth, C.N. Tomé, Twinning Dislocations on {10-11} and {10-13} planes in hcp crystals, Acta Mater. 59 (2011) 3990–4001.
- [76] M. Kronberg, Plastic deformation of single crystals of sapphire: basal slip and twinning, Acta Metall. 5 (1957) 507–524.
- [77] H. Khater, A. Serra, R.C. Pond, Atomic shearing and shuffling accompanying the motion of twinning disconnections in zirconium, Phil. Mag. 93 (2013) 1279–1298
- [78] P.M. Hazzledine, P. Pirouz, Synchroshear transformations in Laves phases, Scr. Metall. 28 (1993) 1277–1282.
- [79] J. Poirier, On the kinetics of olivine-spinel transition, Phys. Earth Planetary Inter. 26 (1981) 179–187.
- [80] A.G. Crocker, The crystallography of deformation-twinning in alpha plutonium, J. Nucl. Mater. 41 (1971) 167–173.
- [81] R.C. Pond, X. Ma, J.P. Hirth, T.E. Mitchell, Disconnections in simple and complex structures, Phil. Mag. 87 (2007) 2307–5289.
- [82] X. San, M.Y. Gong, J. Wang, X. Ma, R. Reis, P.J.M. Smeets, V.P. Dravid, X.B. Hu, Uncovering the crystal defects within aragonite CaCO3, PNAS 119 (2022) e2122218119.
- [83] R.C. Pond, J.P. Hirth, K.M. Knowles, Topological model of type II deformation twinning in NiTi martensite, Phil. Mag. 99 (2019) 1619–1634.
- [84] R.C. Pond, X. Ma, Y.W. Chai, J.P. Hirth, Topological modelling of martensitic transformations, in: F.R.N. Nabarro, J.P. Hirth (Eds.), Dislocations in Solids 13, Elsevier, Amsterdam, 2007, pp. 225–262.
- [85] G.F. Vander Voort (Ed.), Metallography and Microstructure, ASM Handbook, Vol. 9, 2004.
- [86] M.S. Wechsler, D.S. Lieberman, T.A. Read, On the theory of the formation of martensite, Trans. AIME 197 (1953) 1503–1515.
- [87] J.S. Bowles, J.K. Mackenzie, The crystallography of martensite transformations, Acta Metall. 2 (1954) 2815–2822.
- [88] M.S. Wechsler, On the theory of martensite transformations, Acta Metall. 7 (1959) 793–802.

- [89] L.M. Ball, R.D. James, Fine phase mixtures as minimizers of energy, Arch. Rat. Mech. Anal. 63 (1977) 337–403.
- [90] K. Bhattacharya, Microstructure of Martensite, Oxford Univ. Press, Oxford, 2003.
- [91] C.M. Wayman, Introduction to the Crystallography of Martensitic Transformations, Macmillan, NY, 1964.
- [92] P.M. Kelley, L.R.F. Rose, The martensitic transformation in ceramics-its role in transformation toughening, Prog. Mater. Sci. 47 (2002) 463–557.
- [93] R.C. Pond, J.P. Hirth, Response to "The phenomenological theory of martensite crystallography versus the topological model, in: G.B. Olson, D.S. Lieberman, A. Saxena (Eds.), Proc ICOMAT 2008, TMS, Warrendale, PA, 2000, pp. 107–114.
- [94] J.P. Hirth, A dislocation mechanism for phase transformation, in: J.A. Simmons, R. deWit, R. Bullough (Eds.), Fundamental Aspects of Dislocation Theory 1, National Bureau of Standards Special Vol. 317, 1970, pp. 547–552.
- [95] S. Akarapu, H. Zbib, J.P Hirth, Modeling and analysis of disconnections in tilt walls, Scr. Mater. 59 (2008) 265–267.
- [96] S. Amelinckx, Dekeyser W, The structure and properties of grain boundaries, Solid State Phys 8 (1959) 325–499.
- [97] A.H. Clauer, J.P. Hirth, An analysis of L and Y tilt boundary intersections formed during creep in molybdenum, in: Proceedings of the Second International Conference on the Strength of Metals and Alloys III, American Society of Metals, Cleveland, 1970, pp. 1113–1117.
- [98] M. Enomoto, J.P. Hirth, Computer simulation of ledge migration under elastic interaction, Metall. Mater. Trans. 27A (1996) 1491–1500.
- [99] J.W. Christian, Discussion, Metall. Mater. Trans 25A (1994) 1821.
- [100] S.V. Kamat, J.P. Hirth, P. Müllner, The effect of stress on the shape of a blocked deformation twin, Phil. Mag. 73 (1996) 669–680.
- [101] W.Z. Zhang, Decomposition of the transformation displacement field, Phil. Mag. 78A (1998) 913–933.
- [102] Y. Liu, N. Li, S. Shan, M. Gong, J. Wang, R.J. McCabe, Y. Jiang, C.N. Tomé, Characterizing the boundary lateral to the shear direction of deformation twins in magnesium, Nat. Comm. 7 (2016) 11577.
- [103] S.J. Wang, M.Y. Gong, R.J. McCabe, L. Capolungo, J. Wang, C.N. Tomé, Characteristic boundaries associated with three-dimensional twins in hexagonal metals, Sci. Adv. 6 (2020) eaaz2600.
- [104] J.P. Hirth, D.Y. Xie, G. Hirth, J. Wang, Recovery and facets for deformation twins in minerals and metals, PNAS 119 (2023) e2215085120.
- [105] Y. Liu, Z.L. Xie, Twinning and detwinning of <011>type II twin in shape memory alloy, Acta Mater 51 (2003) 5529–5543.
- [106] Z.L. Xie, Y. Liu, HRTEM study of  $\langle 011 \rangle$  type II twin in NiTi shape memory alloy, Phil. Mag. 84 (2004) 3497–3507.
- [107] R.D. Field, D.W. Brown, D.J. Thoma, Texture development and deformation mechanisms during uniaxial straining of U-Nb shape memory alloys, Phil. Mag. 85 (2015) 2593–2609.
- [108] J.R. Rice, Conserved integrals and energetic forces, in: The Eshelby Memorial Symposium, Cambridge Univ. Press, Cambridge, 1984, pp. 33–56.
- 109] B.A. Bilby, A.G. Crocker, The theory of the crystallography of deformation twinning, Proc. Roy. Soc. (London) A288 (1965) 240–255.
- [110] M. Bevis, A.G. Crocker, Twinning shears in lattices, Proc. Roy. Soc. (London) A304 (1968) 123–134.
- [111] J.W. Christian, S. Mahajan, Deformation twinning, Prog. Mater. Sci. 29 (1995)
- [112] A.E. Romanov, M. Hecker, Elastic fields of straight linear Somigliana dislocations near a free surface, phys. stat. sol. (a) 115 (1989) K159–K162.
- [113] A.E. Romanov, W. Pompe, J.S. Speck, Theory of microstructure and mechanics of the...a1/a2/a1/a2... domain pattern in epitaxial ferroelectric and ferroelastic films, J. Appl. Phys. 79 (1996) 4037–4049.